Max-Planck-Institut
für Meteorologie

REPORT No. 119

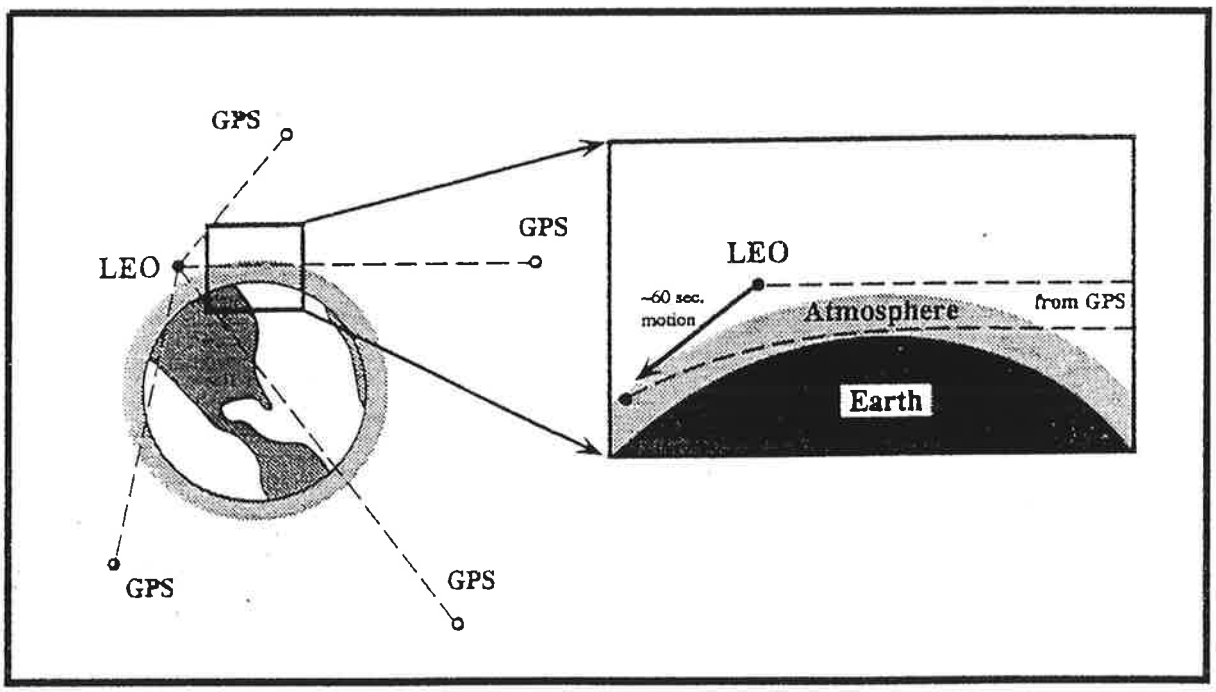

REMOTE SENSING OF REFRACTIVITY FROM SPACE FOR GLOBAL OBSERVATIONS OF ATMOSPHERIC PARAMETERS

by

MICHAEL E. GORBUNOV • SERGEY V. SOKOLOVSKIY

HAMBURG, DECEMBER 1993

AUTHORS:

Michael E. Gorbunov
Sergey V. Sokolovskiy

Russian Academy of Sciences
Institute of Atmospheric Sciences
Pyzhevsky Perenlok 3
109017 Moscow
Russia

MAX-PLANCK-INSTITUT
FÜR METEOROLOGIE
BUNDESSTRASSE 55
D-20146 Hamburg
F.R. GERMANY

Tel.: +49-(0)40-4 11 73-0
Telemail: MPI.METEOROLOGY
Telefax: +49-(0)40-4 11 73-298

Foreword

This paper is a feasibility study on the potential meteorological use of the Global Positioning Satellite System (GPS) carried out by Drs. Gorbunov and Sokolovskiy at the Max-Planck-Institut für Meteorologie. As a substitute for the real atmosphere, simulated data by an atmospheric general circulation model, ECHAM3 at very high horizontal resolution, T106, has been used. The degrees of freedom and synoptic realism do not differ in any significant degree from assimilated data by the ECMWF forecasting model.

The study indicates that the GPS system holds great potential for meteorological use in providing temperature information in particular in the stratosphere and parts of the upper troposphere where the moisture content is low. Alternatively moisture can be retrieved if temperature can be observed by other techniques.

Further work in this area is planned. This will address the computational problem with tomographical retrieval more extensively and explore the effect of clouds, precipitation areas and the handling of discontinuity surfaces such as atmospheric fronts.

Lennart Bengtsson

ISSN 0937–1060

REMOTE SENSING OF REFRACTIVITY FROM SPACE FOR GLOBAL OBSERVATIONS OF ATMOSPHERIC PARAMETERS

Michael E. Gorbunov and Sergey V. Sokolovskiy
Institute of Atmospheric Physics, Russ. Acad. of Sci., Moscow

Abstract

Occultation methods based on effects connected with refraction of electromagnetic waves of both optical and radio frequency domains were numerously used by astronomers for investigations of planetary atmospheres during last decades. Application of these methods for remote sensing of terrestrial atmosphere was delayed essentially due to insufficient possibilities of space based technique to provide necessary accuracy and both temporal and spatial frequency of observations. The successful development of Global Positioning Satellite Systems during the last years on one hand, and plans for launching a great number of Low-Earth Orbit satellites, capable to carry GPS receivers, during the next several years on the other hand, provide an opportunity to create a space radio-occultation system for global observation of atmospheric parameters (pressure, temperature, humidity) and their real-time assimilation together with other observations in Atmospheric General Circulation Models. Among the set of problems connected with the development of such a system is the creation of inversion algorithms that enable to achieve maximum possible accuracy of retrieval of meteorological parameters from refraction data. This problem can be investigated by means of computational simulation prior to the realization of the space system.

This report presents the first results of computational simulations on the retrieval of meteorological parameters from space refractometric data on the basis of the ECHAM 3 model developed at the Max Planck Institute for Meteorology (Roeckner et al. 1992). For this purpose the grid fields of temperature, geopotential and humidity available from the model were interpolated and a continuous spatial field of refractivity (together with its first derivative) was generated. This field was used for calculating the trajectories of electromagnetic rays for the given orbits of transmitting and receiving satellites and for the determination of the quantities (incident angles or Doppler frequency shifts) being measured at receiving satellite during occultation. These quantities were then used for solving the inverse problem - retrieving the distribution of refractivity in the vicinity

of the ray perigees. The retrieved refractivity was used to calculate pressure and temperature (using the hydrostatic equation and the equation of state). The results were compared with initial data, and the retrieval errors were evaluated. The study shows that the refractivity can be retrieved with very high accuracy in particular if a tomographic reconstruction is applied. Effects of humidity and temperature are not separable. Stratospheric temperatures globally and upper tropospheric temperatures at middle and high latitudes can be accurately retrieved, other areas require humidity data. Alternatively humidity data can be retrieved if the temperature fields are known.

1. Introduction

A method for the determination of vertical profiles of refractivity, and further derivation from them of such meteorological parameters as density, pressure and temperature, by measurements of refraction of electromagnetic waves in both optical and radio frequency (RF) domains during transillumination of the atmosphere from space (remote sensing of refractivity) was proposed initially for the investigation of planetary atmospheres (Fjeldbo and Eshleman 1968, Eshleman et al. 1977, Lindal et al. 1981). A classic scheme of sensing is shown in Fig.1. The transmitter and receiver of electromagnetic waves, both situated outside the atmosphere, are moving in such a way that the perigee of a transilluminating electromagnetic ray between both moves in the atmosphere in vertical direction. Different quantities connected with refraction of electromagnetic waves can be measured during such occultations. In the optical domain the incident angle of the ray can be measured with very high accuracy. For the RF domain accurate angular measurements are difficult (they require a very large dimension of the receiving antenna), but it is possible to measure the phase (or Doppler frequency) shift of the signal with extremely high accuracy. These values are connected with each other by simple relations (section 2) and both can be used for solving the inverse problem - retrieving the vertical profile of refractivity in the vicinity of the rays perigees.

The first proposals to apply refractometric occultation methods for remote sensing of terrestrial atmosphere from space were made in the late 60s (Fishbach, 1965; Lusignan et al., 1969). Since in the terrestrial atmosphere the mean distribution of meteorological quantities is known well enough and the purpose is to measure its relatively small variations in order to obtain initial data for weather and climate prediction, it results in more strict requests for the accuracy of measurements. It is aggravated by the fact that refraction effects in the terrestrial atmosphere are very small

(section 3). For many years the capabilities of space based technique for positioning and Doppler measurements were insufficient for solving this problem with acceptable accuracy.

Nevertheless during these years some experiments on remote sensing of refractivity from space were produced in both RF and optical domains (Rangaswamy 1976, Gurvich et al. 1982, Volkov et al. 1987). In the latter two papers the possibility to determine the deviation of refractivity from the mean magnitude was indicated, but it was not possible to answer the question about the real accuracy of the method due to insufficient accuracy of both the remote and the direct measurements.

Along with these experiments some theoretical investigations were done mainly concerned with mathematical aspects of the inverse refraction problem (Douglas et al. 1980, Gurvich and Sokolovskiy 1985, Sokolovskiy 1987, 1990, Gorbunov 1988, 1990, Gorbunov and Gurvich - to appear). These considerations were applied to the 2D tomographical problem, when all soundings are in the same plane. They indicate that the main difficulties in the 2D problem are connected with achieving appropriate horizontal resolution, but for large scale variations of meteorological fields, the potential accuracy of their reconstruction may be sufficient to satisfy existing demands of meteorology and climatology. However, for improving the horizontal resolution in order to reconstruct small scale variations of meteorological fields it is necessary to use a sounding scheme where the viewing for each region is undertaken from different directions. This sounding scheme implies using an iterative tomographical reconstruction algorithm (section 6).

The situation changed radically during the last years due to the successful development of the Global Positioning Satellite Systems (GPS). The GPS includes the distribution of several satellites in polar orbits equipped with radio transmitters with extremely high frequency stability. The positions of the GPS satellites are known with an accuracy of about 1m and the ephemeris are transmitted regularly within special messages. By receiving signals from 4 GPS satellites by a special receiver and comparing the change of their characteristics caused by Doppler effect, one can instantaneously determine the position of the receiver with an accuracy of about 1m. If the observations are taken under conditions when one of the radio links is occulted by the terrestrial atmosphere (see Fig.2) then it is also possible to measure the atmospheric contribution to Doppler data i.e. to obtain initial data for solving the inverse problem of refraction. A single satellite at Low Earth Orbit (LEO) can, with the use of GPS, provide between several hundreds and one thousand

occultations during a day (depending on the height of the orbit) at many points of the globe. As an example, Fig.3 represents on the map of a Northern hemisphere the existing net of standard aerological sounding (radio sounding) together with a net of radio occultations done during a day by 18 GPS satellites and 4 satellites at specially chosen orbits with the height 870 km (Gurvich and Krasilnikova 1990). One can see that in this case the density of radio occultations during a day is approximately the same as the density of the existing radio sounding network over the continents and exceeds the latter considerably over the oceans. At present, it is planned during the next ten years to launch several hundreds of LEO satellites for communication purposes (Hardy et al. 1992). Specially modified GPS receivers may be installed on these satellites. This will make it possible to obtain continuously data on vertical distribution of density, pressure, temperature and probably humidity in the atmosphere all over the globe. The science and technique connected with the development of such a system has been labelled "GPS meteorology" (Ware 1992).

2. The inverse refraction problem.

When treating electromagnetic waves propagation in terms of rays, which is valid for the present problem, then the trajectory of the electromagnetic ray connecting two points can be obtained from the Fermat principle:

$$\int_1^2 n(\boldsymbol{r})\, dl = min \qquad (1)$$

where $n=c/v$ is the refractivity and v and c are the velocities of electromagnetic waves in air and in vacuum respectively.

There are different possible formulations of the inverse refraction problem, depending on peculiarities of the transmitter and receiver motion during observations (Lusignan 1968, Sokolovskiy 1990, Gorbunov 1990, Gorbunov and Gurvich - to appear). It is evident that it is generally impossible to retrieve the 3D distribution of refractivity in the vicinity of the ray perigee from the measured 1D function along the trajectory of the receiving satellite. Some simplifications of the problem are necessary. Here we shall consider the case when transmitter and receiver move such that during the time of occultation, i.e. when the transilluminating ray perigee crosses the atmospheric layer from the surface up to some tens of kilometers height, its horizontal displacement is much smaller than the characteristic horizontal scale of meteorological fields. This

implies that the angle between the line connecting two satellites and the orbital planes of at least one of the satellites should be small. The characteristic horizontal length of interaction between an electromagnetic ray and the atmosphere (see Fig.4) can be defined as $L \cong 2\,(2r_e H)^{1/2}$, $L \cong 600$ km for H=10 km. This value of L is slightly less than the characteristic horizontal scale of meteorological fields. These two reasons make it possible to assume the simplest approximation: to regard the distribution of refractivity as spherically symmetric in the vicinity of the ray perigee $n(\boldsymbol{r}) = n(r)$. Under this assumption the equation for the ray trajectory derived from (1) is given by Snell's law:

$$rn(r)\sin\phi = p \tag{2}$$

where ϕ is the angle between the tangent to the ray and the direction to the center of the Earth, and p is invariant for a given ray, called impact parameter. The total bending angle of the ray $\varepsilon = \int_1^2 dl/\rho_c$ (where ρ_c is the radius of curvature of the ray) called refraction angle, can be expressed by using (3):

$$\varepsilon(p) = -2p\int_p^\infty (dln(n)/dx)\,(x^2-p^2)^{-1/2}dp \tag{3}$$

where $x = r\,n(r)$. The integration in (3) extends to infinity to take into account the fact that both $n(r_1) = n(r_2) = 1$. Expression (3) can be regarded as an integral equation with respect to $n(x)$ and can be solved using the Abel transform:

$$n(x) = exp\,(\pi^{-1}\int_x^\infty \varepsilon(p)\,(p^2-x^2)^{-1/2}dp) \tag{4}$$

where $r=x/n(x)$. Thus if the refraction angle $\varepsilon(p)$ can be measured in some way as a function of the impact parameter of the ray, then the vertical profile of the refractivity $n(r)$ can be retrieved by using (4). In practice the formula (4) is used naturally with the finite upper limit of integration y corresponding to the conventional upper boundary of the atmosphere. This boundary can be defined, for example, from the condition of correspondence of the value ε to the characteristic value of its measuring error, or to the characteristic value of its weather variations. For larger values of p usually the function $\bar{\varepsilon}(p)$ calculated for the standard model of the atmosphere may be used:

$$n(x) = exp\,(\pi^{-1}\int_x^y \varepsilon(p)\,(p^2-x^2)^{-1/2}dp + \pi^{-1}\int_y^\infty \bar{\varepsilon}(p)\,(p^2-x^2)^{-1/2}dp) \tag{5}$$

In this form the inverse refraction problem is well posed i.e. the retrieval error for $n(x)$ can be reduced to any arbitrary value by appropriate reduction of the measurement error for $\varepsilon(p)$.

In the optical domain one can calculate both, the refraction angle ε and, the impact parameter p by measuring the zenith angle of the ray ϕ_1 (see Fig.5) and taking into account the Snell equation (2) from the simple geometrical relations:

$$p = r_1 \sin\phi_1$$

$$\varepsilon = \phi_1 + \phi_2 + \theta - \pi \qquad \text{where} \qquad \phi_2 = arc\sin(p/r_2) \tag{6}$$

In the RF domain, where angular measurements are not available with appropriate accuracy, the function $\bar{\varepsilon}(p)$ may be calculated from Doppler measurements. The doppler shift f_d of the carrier frequency f_0 is given by (see Fig.5):

$$f_d = f_0 c^{-1} (\boldsymbol{n}_1 \boldsymbol{v}_1 - \boldsymbol{n}_2 \boldsymbol{v}_2) \tag{7}$$

By specifying radial and circular components of the satellite velocities in the plane coinciding with the ray trajectory as v^r and v^c and taking into account the Snell equation (2) one can calculate angles ϕ_1 and ϕ_2 from the following relations:

$$f_d = f_0 c^{-1} (v_1^r \cos\phi_1 + v_2^r \cos\phi_2 + v_1^c \sin\phi_1 - v_2^c \sin\phi_2) \tag{8}$$

$$r_1 \sin\phi_1 = r_2 \sin\phi_2$$

Finally, $\bar{\varepsilon}(p)$ can be calculated by using (6).

Thus Doppler and angular data are connected by simple relations and both may be used for solving the inverse refraction problem. The result will be the same in the case of single ray propagation, that is valid for observations from Low-Earth Orbits.

3. Refraction properties of the terrestrial atmosphere.

The refractivity of air in the RF domain can be given by simplified formula, (Bean and Datton, 1968):

$$n - 1 = c_1 P/T + c_2 P_w/T^2 \qquad (9)$$

where: P and P_w are total pressure of air and pressure of water vapor respectively, T is temperature and $c_1 = 7.76 \cdot 10^{-5}$(K/mb), $c_2 = 3.73 \cdot 10^{-1}$(K^2/mb). In the optical domain the second term in (9) can be neglected. The refractivity of air is very close to unity, it differs from unity by $\sim 3 \cdot 10^{-4}$ near the terrestrial surface and this difference decreases exponentially with height. The refraction angle e for the ray touching the terrestrial surface is of the order of $\sim 2 \cdot 10^{-2}$ rad and decreases also exponentially with the height of the ray perigee.

Fig.6 shows the function $\varepsilon(p)$ for one of the vertical profiles of refractivity calculated from the T106 model grid data (a lay-out of computations will be given below). One can see the characteristic bump on the curve, corresponding to the tropopause. Fig.6b shows the Doppler shift f_d as a function of time during occultation for a carrier frequency of $f_0 = 1.5$ GHz and a circular orbit of the LEO satellite at 250 km height. As it can be seen from Fig.6b, the atmospheric input to Doppler shift (~200Hz for the ray touching the terrestrial surface) is a small contribution to the shift in vacuum, which is defined by the relative motion of the satellites. Note that the tropopause is also visible on the Doppler curve.

In practice, for measuring such a small input in frequency, taking into account that it changes with time, the frequency is reduced by heterodyning and the phase change of the low frequency output signal is measured by counting zeros of the signal and assuming that the phase change between them is equal to π. Then the phase may be interpolated as stepwise function of time and differentiated to obtain frequency. An alternative way may be to fit a low frequency signal by some analytical function (to reduce the influence of noise) and then to count zeros.

At 30 km altitude the characteristic value of the refraction angle is about $4 \cdot 10^{-4}$ rad, and the corresponding value of the Doppler shift is about 4Hz. If we set a goal to measure refractivity (meteorological parameters) at 30 km altitude with 0.1% accuracy then it is necessary to measure angles with an accuracy of $4 \cdot 10^{-7}$ rad, and Doppler shift with an accuracy of $4 \cdot 10^{-3}$Hz, which is possible if the relative stability of frequency is no worse than 10^{-12}. Besides this, a relative refractivity error of 0.1% for the given height corresponds to an absolute height error of 1m for the given refractivity. This indicates that absolute values of the impact parameter p, and therefore the positions of satellites in the coordinate system connected with the Earth, must be known with the same accuracy. Such high requirements to the accuracy of refraction data in the terrestrial

atmosphere were among the reasons for postponing development of the space radio occultation technique for global observations of atmospheric parameters.

4. The use of GPS for Doppler measurements

The GPS satellites are located in circular polar orbits at a height of 20183 km such that in each moment at any arbitrary point on earth at least 4 satellites can be observed simultaneously above the horizon. They carry transmitters at frequencies 1227.6GHz and 1575.42GHz with very high stability of the carrier frequencies (about 10^{-12}) (Parkinson 1983). Such high stability of the frequency makes it possible to determine the relative velocity between satellites by measuring the Doppler frequency shift with an accuracy of up to 0.1 mm/sec. The carrier frequencies are modulated by special pseudo-random codes for ranging and special navigation messages including information about orbital parameters. By measuring the delay time for a definite phase of the code the pseudo-range between the receiver and the GPS satellite is calculated. By measuring pseudo-ranges for 4 satellites the position of the observer is determined (practically instantaneously) with an accuracy of up to 1m in the coordinate system of the Earth.

For radio occultation sounding of the atmosphere (see Fig.7) the positioning of the receiving satellite can be done just before the occultation of one of the four GPS satellites. During the occultation it is necessary to measure Doppler shifts of the carrier frequencies in all four radio-links. The frequency shift of the occulted radio-link serves as initial data for the calculation of $\varepsilon(p)$ as described above. The three frequency shifts of the non-occulted radio-links enable to calculate with sufficient accuracy the velocity vector $v_1(t)$ of the receiving satellite in order to use it along with $f_d(t)$ for calculation of $\bar{\varepsilon}(p)$.

Thus, the accuracy of positioning and frequency stability of GPS is sufficient for measuring refraction effects with an accuracy of 0.1% for altitudes up to 30 km. But this accuracy can only be fully realized in the case of a spherically-symmetric distribution of refractivity. The approximate character of the solution of inverse refraction problem by Abelian inversion will result in some additional retrieval errors to be investigated (section 5). To overcome these errors it is necessary to use tomographic reconstruction including data from different view directions (section 6).

5. Computational simulation of the retrieval of refractivity and meteorological parameters by an Abelian inversion on the base of the T106 model.

The main goal of computational simulation of the retrieval of meteorological parameters from remote sensing of refractivity is the estimation of the retrieval errors, connected with the approximate character of the solution of the inverse refraction problem before the instrumental realization of the method. Computations were made using the realization of meteorological fields from the data bank of the T106 model, corresponding to the date: March 1, 1988, time: 12 GMT.

The computational simulation consists of the following main parts:

1) Exact solution of the direct refraction problem and calculation of quantities being derived from Doppler data. This solution is produced for the 3D distribution of refractivity calculated on the basis of grid fields available from the T106 model (The ECHAM3 Atmospheric General Circulation Model 1993), and for given orbital parameters of GPS and LEO satellites. As a result of this step grid functions $\bar{\varepsilon}(p)$ are calculated.

2) Approximate solution of the inverse refraction problem (by Abelian inversion) and retrieval of the grid vertical profiles of refractivity. Derivation of the meteorological quantities (pressure and temperature) from the retrieved refractivity profiles.

3) Comparison of the retrieved meteorological parameters with ones in the vicinity of transilluminating ray perigees and calculation of retrieval errors.

5.1. Solution of the direct refraction problem.

The solution of the direct refraction problem results in the numerical integration of the exact equations for the trajectories of the rays connecting transmitter and receiver at different times during the occultation. These equations can be derived from (1). In the general 3D case the trajectory of the ray can not be regarded as on plane curve. But as it was shown by Lusignan et al. 1969, the horizontal component of the gradient of refractivity normal to the plane defined by the satellites and the Earth's center may be ignored as it results in negligibly small corrections to angular and Doppler data. So it is enough to take into account a gradient of refractivity in the mentioned plane. In this case the equation for the ray trajectory $r(\theta)$ derived from (1) will be:

$$d^2r/d\theta^2 =$$

$$r + 2\,(dr/d\theta)^2/r + [\partial n/\partial r - (dr/d\theta)\,(\partial n/d\theta)/r^2]\,[r^2 + (dr/d\theta)^2]/n\,(r,\theta) \qquad (10)$$

This equation is non-linear with respect to $r\,(\theta)$ and for finding the trajectory connecting the two given points one has to use the shooting method. To reduce the computational time we shall assume here that the orbital plane of the LEO satellite coincides with one of the GPS satellites (see Fig.8a). In this case we can regard all the rays during the occultation to be situated in one and the same plane coinciding with the orbit of the LEO satellite. This enables us to avoid the shooting method, but instead integrate each ray once for a given value of the impact parameter at the transmitting point, and then to calculate the point of intersection between the ray and the orbit of the LEO satellite (see Fig.8). In this case the time grid will not be uniform but this does not pose any difficulties. This simplification will not influence the results in a major way because in order to use the Abelian inversion for processing the experimentally measured data the angle between the direction to GPS and the orbital plane of LEO satellite was already required to be small (section 2.).

For the numerical integration of equation (10) by a Runge-Kutta method it is generally necessary to continuously interpolate refractivity together with first derivatives at arbitrary points. In order to avoid calculations of refractivity and its derivatives for each integration step by complicated interpolation formulas and to reduce computational time, it is possible to precalculate continuous vertical profiles of refractivity (together with its vertical and horizontal derivatives) for the uniform grid $n\,(r, \theta_i)$ and to use this grid for the integration of all rays for one occultation with constant step $\Delta\theta = \theta_{i+1} - \theta_i$ (see Fig.9). The value of the step $\Delta\theta$ was taken to be $2.5 \cdot 10^{-3}$rad that corresponds to ~16 km along the terrestrial surface.

Integration of each ray was taken up to an altitude of 200 km, corresponding to the altitude of the LEO satellite (above 200 km it was considered to be a straight line). At the end of integration the refraction angle ε and impact parameter p were calculated according to (6). The sets of ε and p values calculated for different rays during one occultation formed the grid function $\varepsilon\,(p)$. The step along p was taken about 0.1 km.

5.1.1. Continuous interpolation of density and refractivity.

To reduce the computational time the "gaussian" grid, used in the T106 model, was replaced by a simplified uniform grid with meridian step 1.121457° counted from the latitude 89.155866°. Both these values were defined from minimum rms deviation of the "gaussian" latitudes from the uniform ones. The rms deviation is about 0.002° and the maximum deviation about 0.015°, so that horizontal distortions of meteorological fields due to such a grid substitution are negligibly small.

As the vertical profile in the T106 model is not continuous in temperature and does not provide continuity of derivatives for pressure and humidity, it is not suitable for computations of ray trajectories. It is not possible to use separate continuous interpolations for pressure, temperature and humidity, as this will be inconsistent with the equations of state and the hydrostatic equation. The way is to interpolate continuously in density, then to derive pressure and virtual temperature and to regard them as reference profiles instead of those from the model. The problem is to interpolate density in such a way that the derived pressure and virtual temperature would be close to the T106 model values at half and full levels. The scheme of chosen interpolation is shown in Fig.10.

Geopotential heights z_g for both half and full levels were recounted in advance to metric heights: $z = z_g / (1 - z_g / r_e)$ and namely metric units are used further.

The temperature T was linearly interpolated between full levels, while $\log(P)$ and $\log(q)$ where P is pressure and q is specific humidity) were interpolated between half levels. Then density ρ and refractivity n were calculated at the levels of uniform vertical grid with a step of 1 km up to 35 km. For the uniform layer between the 1st T106 level and 35 km the temperature was considered to be constant corresponding to the 1st T106 full level and humidity q=0.

The vertically uniform grid profiles of $\log(\rho)$ and $\log(n-1)$ were calculated for each point of the simplified uniform geographic grid. Then they were linearly interpolated horizontally into the points θ_k in the plane of the ray trajectories (see Fig.9). The difference $\theta_{k+1} - \theta_k$ was taken to be $2 \cdot 10^{-2}$ rad that corresponds to the horizontal resolution of about 125 km in the T106 model. In this plane they were interpolated between θ_k by cubic splines, and at each point θ_i the vertical grid profiles of $\log(\rho)$, $\log(n-1)$, $\partial \log(\rho)/\partial\theta$, $\partial \log(n-1)/\partial\theta$ were calculated. Then all these profiles for each point θ_i were interpolated along the vertical direction by cubic splines and

extrapolated above 35 km linearly using the values and slopes at 35 km. Thus, an array of spline coefficients was obtained which enables a fast computation of density and refractivity along with derivatives while integrating the ray trajectories.

An example of the reference continuous virtual temperature profile derived from the density profile for the T106 model grid field is shown in Fig.11. It can be seen that the deviation from the T106 model grid values is larger when the characteristic vertical scale of temperature inhomogeneities is comparable with the vertical step of the T106 model. The rms deviation does not exceed 1 K while maximum deviation may be about several K. Naturally the results of temperature and pressure retrieval will be compared with the derived continuous profiles.

5.2. Solution of the inverse refraction problem and calculation of the meteorological quantities.

The inverse problem for the computed function $\varepsilon(p)$ was solved for each occultation by Abelian inversion under the assumption of the local spherical symmetry of refractivity distribution in the sufficient vicinity of the ray perigee, as was described above:

$$n(x) = exp\left(\pi^{-1}\int_x^y \varepsilon(p)\,(p^2 - x^2)^{-1/2} dp\right) \tag{11}$$

Then the retrieved refractivity n was expressed as a function of $z = x/n(x) - r_e$. The value y refers to the conventional upper boundary of the atmosphere at 200 km height.

The further computation of meteorological parameters from the retrieved refractivity under conditions when no additional data is available can be made under the assumption of dry air. Then density ρ can be derived from refractivity n by using (9):

$$\rho(z) = [n(z) - 1]/c_1 R \tag{12}$$

where R is the gas constant for dry air. Pressure P and temperature T are derived from density ρ by using the state and hydrostatic equations:

$$P(z) = \int_z^{y - r_e} g(z')\,\rho(z')\,dz' \tag{13}$$

$$T(z) = P(z)/R\rho(z) \tag{14}$$

All the retrieved profiles are gridded ones with non-uniform height step about 0.1 km. To calculate the geopotential heights from the pressure profile a linear interpolation was used.

The perigees for the rays touching the terrestrial surface and passing at 30 km altitude have some horizontal shift of about 70 km, (see Fig.8) which is not large in comparison with the size of the grid cell of the T106 model. The retrieved vertical profiles for each occultation were considered to be valid for the point with the geographical coordinates of the perigee of the ray passing at 10 km altitude.

The control computation was produced with a spherically symmetric exponential profile of refractivity:

$$n(z) - 1 = \alpha exp(-z/H) \tag{15}$$

where $\alpha = 3 \cdot 10^{-4}$, $H = 7.5$ km showed that the full retrieval computation error for the closed circuit (direct problem + inverse problem) does not exceed for refractivity $\sim 4 \cdot 10^{-9}$ (near the terrestrial surface), for temperature and geopotential heights (under the assumption of dry air) $\sim 2 \cdot 10^{-3} K$ and ~8cm, respectively, in the height interval 0-30 km.

5.3. Comparison of the retrieved temperature and geopotential with the reference values.

In order to separate pressure and temperature errors connected with the errors of refractivity retrieval (due to the approximate character of the solution of the inverse refraction problem) from errors connected with the fact that humidity is not taken into account at the stage of pressure and temperature calculation from refractivity, the results are represented below in the following way. At the left halves of the Figs.12-15. there are given vertical temperature profiles {1} derived from virtual refractivity: $n_v - 1 = 7.76 \cdot 10^{-5} P/T_v$, where $T_v = T(1 + 0.608q)$ is the virtual temperature, and these {2} derived from RF refractivity: $n - 1 = 7.76 \cdot 10^{-5} P/T + 3.73 \cdot 10^{-1} P_w/T^2$ (the difference between these profiles has nothing to do with the retrieval of refractivity). At the right halves the differences in temperatures are given calculated from retrieved refractivity profiles and from the local ones in the vicinity of the ray perigees (the same: {1} for virtual refractivity, and {2} for RF refractivity). The differences result from the horizontal inhomogeneity of meteorological fields and of refractivity in the atmosphere. The values retrieved under the assumption of locally spherical symmetry are horizontally averaged

along the scale L in the vicinity of the rays perigees. The smaller the characteristic horizontal scale of inhomogeneities of the meteorological fields in the vicinity of the ray perigees the larger retrieval errors may be. The retrieval error {1} is approximately the same that it would be while using the optical domain. The total errors for the RF domain can be obtained by summarizing the errors {2} at the right halves with the differences between {2} and {1} at the left halves. The geopotential heights and their retrieval errors given in Figs.12-15 have the same meaning at the left and right halves as those for temperatures.

As it can be seen from Figs.12-13, for middle latitudes a noticeable error in temperature and geopotential due to water vapor occurs at altitudes lower than 5-7 km. The retrieval errors due to horizontal inhomogeneity are approximately the same for virtual (optical) and RF refractivity that indicates that characteristic horizontal scales for temperature and humidity inhomogeneities are of the same value. For polar regions (Fig.14) both the errors due to humidity and due to horizontal inhomogeneity are smaller. For tropical regions (Fig.15) the situation differs considerably. The temperature and geopotential errors due to humidity become essential at altitudes below 12 km and are very large near the surface. The retrieval errors due to horizontal inhomogeneity are very small in the troposphere when using virtual (optical) refractivity, which indicates the fact that the horizontal structure of the temperature field is very smooth. On the contrary, retrieval errors in troposphere in the case of using RF refractivity are rather large. That indicates the strongly inhomogeneous horizontal structure of the humidity field.

6. Computational simulation of the tomographical retrieval of refractivity and meteorological parameters on the base of the T106 model

6.1. Data interpolation

The data interpolation algorithms include two groups of algorithms:

1) interpolation of initial data of the T106 model to uniform spatial grid;

2) interpolation of meteorological fields from the uniform spatial grid to an arbitrary point.

The algorithms of the first group were used for preparing data sets for numerical modeling of remote sensing of the atmosphere. The algorithms of the second group were used when tracing the rays through the atmosphere.

6.1.1. Interpolation of T106 data to a uniform spatial grid

The initial data for interpolation were arrays of:

1) geopotential at the half levels $\phi_{k+1/2}$, k =0, 1, 2 ... 18

2) surface geopotential ϕ_s

3) surface pressure P_s

4) temperature at the full levels T_k, k=1, 2, 3 ... 19

5) humidity (water vapour mixing ratio) at the full levels $(q_V)_k$, k = 1, 2,3 ... 19

For all the vertical profiles the uniform height grid was stated:

$z_i = i\Delta z$, i = 0..26, Δz = 1.5 km

The calculation of vertical profiles of density and humidity on this grid was done in the same way as described above (see section 5.1).

The next procedure was horizontal interpolation in order to use a uniform latitude grid rather than a gaussian grid, as in the T106 model. For this purpose the natural cubic spline interpolation with respect to latitude was used.

Thus 3D arrays of density and humidity were calculated, each point of which, say ρ_{ijk}, corresponds to i-th height level z_i above the surface point θ_j, φ_k, where latitudes (counted from the North Pole)

$$\theta_j = j\Delta\theta, j = 0..N$$

and longitudes

$$\varphi_k = k\Delta\theta, k = -N..N,$$

$$N = 160,\ \Delta\theta = \frac{180^\circ}{N}$$

This network was enlarged so that the indexes j and k would change in a greater range:

$$j = -\Delta N..N + \Delta N$$

$$k = -N - \Delta N..N + \Delta N,$$

where $\Delta N = 10$. It was done according to the definitions:

1) indexes $k' = N + \Delta k$ and $k'' = -N + \Delta k$ are equivalent, where $\Delta k = -\Delta N..\Delta N$

2) surface points $(j', k') = (-\Delta j, k)$ and $(j'', k'') = (\Delta j, k - N \text{ sign } k)$ are equivalent;

3) surface points $(j', k') = (N + \Delta j, k)$ and $(j'', k'') = (N - \Delta j, k - N \text{ sign } k)$ are equivalent. (The function sign k is equal to -1 for $k < 0$ and 1 otherwise.)

Enlarging the network allowed acceleration of the interpolation of the fields to an arbitrary point, as it will be explained below.

6.1.2. Interpolation of the refractivity field to an arbitrary point

Interpolation of the refractivity field to an arbitrary point is necessary for tracing radio rays through the atmosphere. The ray-tracing procedure will be described below. The procedure of interpolation of refractivity was based on using natural cubic splines.

The procedure of spline interpolation is linear with respect to a set of values f_i, and therefore, the spline $\tilde{f}$ is linear combination of "δ-splines":

$$\tilde{f}(x) = \sum f_i S_i(x),$$

where S_i is a spline, which forms 1 at x_i and 0 at other grid points.

If the grid is x_i equidistant, and if the point x is far enough from the end of the interval of interpolation, then the dependence of the form of S_i function on index i may be neglected. Thus the interpolated function may be represented in the form similar to the Shannon - Kotelnikov expansion (Natterer 1986):

$$\tilde{f}(x) = \sum f_i S(x - x_i).$$

For the infinite interpolation interval this formula is exact, and this series converges far faster than the Shannon - Kotelnikov series. It may be represented approximately by its finite part, then the summation index will change in the interval $i(x) - \Delta N \,..\, i(x) + \Delta N$, where $i(x)$ is the index of the grid point nearest to x. The same formula may be used for a finite interpolation interval, if the point x is located at the distance more than $\Delta N \; \Delta x$ from its ends, where Δx is the grid step.

If we have a 2D equidistant rectangular grid (x_i, y_i) and an array of function values f_{ij}, than we can write a similar interpolation formula:

$$\tilde{f}(x, y) = \sum f_{ij} S(x - x_i) S(y - y_i).$$

A similar formula may be written for the derivatives of $\tilde{f}$, for example,

$$\tilde{f}'_x(x, y) = \sum f_{ij} S'_x(x - x_i) S(y - y_i).$$

The procedure of interpolation of refractivity was as follows. The values of $w = \ln(n - 1)$ were interpolated rather than the values of n, because vertical profiles of w are close to linear. At first step the linear vertical trend $w_0(z)$ was subtracted from w:

$$\Delta w(z, \theta, \varphi) = w(z, \theta, \varphi) - w_0(z).$$

Then for the calculation of $\Delta w(z, \theta, \varphi)$ the vertical profile of values $\Delta\tilde{w}(z, \theta, \varphi)$ was calculated using the interpolation formula. The enlarged grid domain (see above) allowed to use the interpolation formula at any surface point. Then this vertical profile was spline-interpolated, giving the value $\Delta\tilde{w}(z, \theta, \varphi)$. The derivatives of $\tilde{w}$ were calculated similarly, using the derivatives of the spline.

The ray tracing technique requires the refraction index for heights greater than the upper bound of the vertical grid used. For the points above the upper most grid level the logarithm of refractivity w was linearly extrapolated up to the conventional height of the atmosphere, which was set to be equal 120 km.

The ray tracing procedure operated with cartesian coordinates rather than with spherical. The North and South poles are the singular points of the coordinate system, but for the sake of saving computing time no checking for this points was made in the programs, but for numerical calculations regions were chosen which did not contain these points.

6.2. Solution of the direct problem

6.2.1. Ray trajectory equations

The equations of the rays are derived from the principle of minimum action. If a refractivity field $n(\boldsymbol{x})$ is given, where $\boldsymbol{x} = (x^1, x^2, x^3)$ is a set of coordinates, then the rays minimize the functional:

$$\Phi = \int L(\boldsymbol{x}, \dot{\boldsymbol{x}})\, d\tau,$$

$$L = n(\boldsymbol{x})\, |\dot{\boldsymbol{x}}|,$$

where τ is the parameter of the trajectory: $\boldsymbol{x} = \boldsymbol{x}(\tau)$.

The simplest form of ray trajectory equations may be obtained in cartesian coordinates when choosing the parameter τ so that $d\tau = \frac{ds}{n}$, where s is the ray arc length. Under this conditions

$$L = n(\boldsymbol{x}) \sqrt{(\dot{x}^1)^2 + (\dot{x}^2)^2 + (\dot{x}^3)^2},$$

and the Euler - Lagrange equation:

$$\frac{d}{d\tau}\frac{\partial L}{\partial \dot{x}^i} - \frac{\partial L}{\partial x^i} = 0$$

takes the form

$$\frac{d^2\boldsymbol{x}}{d\tau^2} = n\frac{\partial n}{\partial x^i}.$$

This equation may be rewritten as a system of the first order:

$$\frac{d\boldsymbol{x}}{d\tau} = \boldsymbol{u}$$

$$\frac{d\boldsymbol{u}}{d\tau} = n\frac{\partial n}{\partial x^i}.$$

6.2.2. Numerical algorithms for the solution of the direct problem

The numerical algorithm for the solution of the direct problem is based on a finite step integration of the ray trajectory equation using the Runge - Kutta method.

If we state the initial conditions for a ray: $\boldsymbol{x}(0) = \boldsymbol{x}_0$, $\boldsymbol{u}(0) = \boldsymbol{u}_0$, then we can integrate the ray trajectory equation until the ray leaves the atmosphere. The refraction is calculated as the angle between the directions of the start and the final ray.

For finding a ray connecting two given points a numerical algorithm was elaborated based on the dichotomical procedure, which is a solution method for the equation:

$$f(x) = 0$$

At each step of solving this equation there are two values x_+ and x_- at which the function f is positive and negative respectively. Then the new value $x = (x_+ + x_-)/2$ is tested. If $f(x)$ is positive (negative) then this value is assigned to x_+ (x_-). It is clear that each step decreases twice the interval in which the solution is, and the solution may be found with any given accuracy.

For finding a ray between two given points a ray tracing procedure was written which stops ray-tracing in the point nearest to the desired ray destination and calculates the difference $\boldsymbol{d}$ between the end of ray point and the destination point. Introducing the orthonormal basis $\boldsymbol{l}$, $\boldsymbol{n}$, $\boldsymbol{b}$, where $\boldsymbol{l}$ is the ray direction at the start ray point to its destination, $\boldsymbol{n}$ lies in the vertical plane, and $\boldsymbol{b}$ is a horizontal vector, we may write the conditions for the ray at the desired destination:

$$(\boldsymbol{d}, \boldsymbol{n}) = 0;$$

$$(\boldsymbol{d}, \boldsymbol{b}) = 0.$$

$\boldsymbol{d}$ is treated as a function of the initial conditions of the ray. We must find the initial direction of the ray, which is defined by the starting value of the vector $\boldsymbol{u}$. The vector $u_0 = \left.\frac{dx}{d\tau}\right|_{\tau=0}$ is defined by two values, say $u_0^2 = (\boldsymbol{u}_0, \boldsymbol{n})$ and $u_0^3 = (\boldsymbol{u}_0, \boldsymbol{b})$, because its third component $(\boldsymbol{u}_0, \boldsymbol{l})$ is known and always equal to $\left.\frac{ds}{d\tau}\right|_{\tau=0} = n(\boldsymbol{x}_0)$. As a first step of the solution of this system its first

equation was solved using the dichotomical method, with respect to u_0^2 with a zero value of u_0^3. At the second step the second equation was solved with respect to u_0^3 with u_0^2 being equal to its previously found value. Then the first equation was solved again with respect to u_0^2 with the previously found u_0^3. This iterations were repeated until $|\boldsymbol{d}|$ became less than a stated accuracy.

In practice it was found to be necessary to test about 30 rays for finding a ray between two given points, if the required pointing accuracy of the ray at the destination is 10 cm.

6.2.3. Scheme for the generation of an atmospheric sounding

A simplified scheme of atmospheric sounding was used. Above each surface point the refraction profiles were calculated in a vertical column. The algorithm was as follows.

For a given surface point characterized by a unit vector $\boldsymbol{x}_p$, the satellite location was calculated using the formula:

$$\boldsymbol{x}_s = R_e \boldsymbol{x}_p + D_s \boldsymbol{l},$$

where D_s is the distance to the satellite (26000 km) and $\boldsymbol{l}$ is direction to the satellite which should be perpendicular to $\boldsymbol{x}_p$.

For the calculation of the vertical profile of refraction, the height levels were specified as:

$$h_i = i\Delta h, i = 0..N_h$$

and the rays were traced with starting direction from point $\boldsymbol{x}_s$ to points $(R_e + h_i)\,\boldsymbol{x}_p$. The height step is $\Delta h = 1$ km, and the number of heights is $N_h = 40$. For greater heights the logarithm of the refraction angle profile was linearly extrapolated.

For providing sufficient horizontal resolution, it is necessary to have data for several viewing directions $\boldsymbol{l}$, so this calculations were repeated for different vectors $\boldsymbol{l}$, calculated from each other by turning around the surface point vector $\boldsymbol{x}_p$.

The number of viewing directions may be estimated as the ratio of the resolution for the approximation of local spherical symmetry (this is the characteristic scale of averaging of

atmospheric fields, about 600 km) to the desired resolution which equals twice the grid spacing, i.e. about 200 km. Thus the estimation of the number of viewing directions is 3.

6.3. Algorithm of solution of the inverse problem

The solution of the inverse problem was based on the numerical algorithm, which is a modification of Kaczmarz's method (Natterer 1986), widely used for solving tomographical problems. The scheme of the algorithm is as follows.

Several sets of refraction angles are given, each of them corresponding to one viewing direction. Let us denote each set of refraction angle profiles above each surface point with ε_j, where the index j refers to the directions.

For each viewing direction we can write a rough approximation of the inverse operator in the form of Abel's inversion. If $\varepsilon_j(\boldsymbol{x}_p, p)$ is a refraction angle profile above the surface point $\boldsymbol{x}_p$, corresponding to the j-th viewing direction ($\boldsymbol{x}_p$ is a unit vector), then Abel's inversion may be approximately written as:

$$n(x) = \frac{1}{\pi}\int_x^\infty \varepsilon(p)\frac{dx}{\sqrt{p^2 - x^2}}$$

where x is the refractive radius, which is connected with the usual radius r by the relation: $x = rn(r)$. This relation may be used for calculating the profile $n(r)$ from $n(x)$. The reconstructed vertical profile should then be treated as the profile above the surface point $\boldsymbol{x}_p$, i.e. $n(r\boldsymbol{x}_p)$. Let us denote Abel's inversion operator as $\hat{A}$. If we use the refractive radius x instead of r, then Abel's inversion provides on linear transform, connecting the refraction angle and the refractivity profiles.

Abel's inversion is exact for a spherically-symmetrical field, but for the 3D problem it was used only as an approximate inversion in the iterative process.

The iterative procedure is as follows. The initial approximation $\tilde{n}_0$ of the refractivity field was calculated as Abel's inversion of the average refraction angle profile. Let us denote $\hat{D}_j$ as the solution operator of the direct problem for j-th viewing direction. Then for each j we can calculate the next approximation using the formulas:

$$\tilde{\varepsilon}_j = \hat{D}_j \tilde{n}_{j-1}$$

$$\tilde{n}_j = \tilde{n}_{j-1} + \hat{A}\,(\varepsilon_j - \tilde{\varepsilon}_j)\,.$$

Thus we see, that on each step the difference between the measured refraction and the refraction calculated for the current approximation is used for the correction of the approximate refractivity field. This procedure may be repeated until the difference $\varepsilon_j - \tilde{\varepsilon}_j$ becomes sufficiently small.

6.4. Calculation of meteorological fields from refractivity

The refractivity n is related with pressure P, temperature T and humidity q_v by the formula:

$$n = 1 + 0.776 \cdot 10^{-6} \frac{P}{T} + 0.373 \cdot 10^{-2} \frac{e}{T^2},$$

where e is the water vapour pressure:

$$e = \frac{P q_v}{\varepsilon + (1-\varepsilon)\, q_v}.$$

In the absence of humidity the refractivity is a linear function of density, which is proportional to $\frac{P}{T}$ due to the thermodynamic equation of state.

$$\rho = \frac{P}{R_d T}.$$

The vertical profile of density determines the pressure profile from the hydrostatic equation:

$$P(z) = \int_z^{\infty} g(z')\,\rho(z')\,dz'$$

Pressure and density allow the calculation of the temperature :

$$T = \frac{P}{R_d \rho}.$$

If the humidity is not zero then the refractivity field does not determine the meteorological fields, and additional data should be used.

In our numerical tests the meteorological fields were calculated as if the humidity was absent. The reconstruction error was calculated in two different ways:

1) the reconstructed meteorological fields were compared with reference ones;

2) the reconstructed meteorological fields were compared with ones calculated from reference refractivity under the assumption that humidity is zero ("dry fields").

The first way of calculation of errors allowed understanding at what heights and where humidity is essential. The second way allowed estimation of errors of reconstruction of pressure and temperature, which would occur if humidity is known.

6.5. Discussion of results of tomographical reconstruction

Numerical tests were done for two limited regions:

1) subequatorial region (11.25° N - 11.25° S, 11.25° W - 11.25° E);

2) European region (39° N - 68° N, 0° E - 28° E).

Figures 20-31 represent the initial fields and the reconstruction error for reference and dry fields.

The error maps show that maximum errors occur near the boundaries. This is due to the fact that the field being reconstructed should be extrapolated outside the region because the viewing rays pass through a wider region. Thus the error near the boundary "compensates" the extrapolation error so that the calculated refraction for the rays would be the same as measured. This problem will not arise if the region investigated is the whole globe.

Thus the representative error values should only be considered far enough from the boundaries.

For the subequatorial region the characteristic geopotential error for the pressure levels 20 and 70 mbar is about 20 - 40 cm and the temperature error is about 0.05 K. At a pressure level of 200 mb (which corresponds to the height about 12.5 km) the influence of humidity becomes more sensible and the error of geopotential increases to 2 - 5 m and temperature error increases up to 0.5 - 1 K. At lower levels this errors are greater, and at the Earth's surface they are very big: geopotential error - about 500 m, and temperature error - about 70 K. But "dry" errors at this levels remain in the same limits as at high levels. Thus it is essential to take humidity into account for the reconstruction of meteorological parameters in the troposphere.

For the European region an improved solution algorithm of the inverse problem was used. On each step of the iterative process the reconstructed field was linearly extrapolated to a slightly greater region then one investigated in order to reduce the errors near the boundaries.

The figures show that the geopotential error for the European region is about 0.5 - 1 m, and temperature error is about 0.05 K for dry fields. The influence of humidity becomes significant at lower levels than in the subequatorial region. For the European region humidity should be taken into account in the height range 0 - 8 km. Thus for pressure levels 20, 70, 200 mbar which are presented on the figures the influence of humidity is insignificant.

7. The possibility for deriving tropospheric humidity from refractivity and temperature.

As can be seen from Fig.15, the error of temperature retrieval from RF refractivity due to tropospheric humidity may be unacceptably large. To retrieve temperature it is necessary to use additional data about humidity. Another possibility is to determine humidity taking into account temperature data.

Let us assume that both RF refractivity $n(z)$ and temperature $T(z)$ profiles are known. Then the specific humidity profile $q(z)$ can be derived by the following iterative procedure.

1) Assumption that the air is dry: $q(z) = 0$

2) Computation of the virtual temperature profile: $T_V(z) = T(z)\,[1 + 0.608 q(z)]$

3) Computation of the pressure profile $P(z)$: $P(z) = P(z^*)\, exp\,[R^{-1} \int_z^{z^*} g(z')\, T_v^{-1}(z')\, dz']$

4) Computation of the specific humidity profile $q(z)$:
$P_w(z) = T(z)^2\,[n(z) - 1 - c_1 P(z)/T(z)]/c_2$
$q(z) = 0.622 P_w(z) / [P(z) - 0.378 P_w(z)]$

5) Return to step 2)

This iterative procedure converges quickly; after the second step the change of $q(z)$ is less than 1%. As an example, Fig.32 shows the temperature profile taken from the T106 model downwards from the 7 full level and interpolated linearly between half and full levels. Along with temperature the specific humidity profile as retrieved by the iterative procedure described above using the RF

refractivity profile calculated beforehand, is shown. Solid lines refer to reference profiles, while dashed line profiles show the influence of systematic and pseudo-random temperature measuring errors.

Above the ocean areas independent temperature measurements are not so reliable as over land, but the water surface temperature may be measured by passive microwave sounding from satellites. In this case it is possible to interpolate the temperature linearly between the surface and the lowest level at which it is derived from RF refractivity with acceptable accuracy (approximately 200mb in tropics), and to use the iterative procedure described above for the determination of the surface pressure of water vapor. The simulation on the base of the T106 model with the tropical area of the Pacific Ocean ($-22.5° \div 22.5°$ latitude, $152° \div 252°$ longitude) shows the following. The mean surface pressure is $\langle e \rangle \cong 27.8$ mb, the mean error of its determination is $\langle \delta e \rangle \cong 1.55$ mb, while the rms error $\langle \delta e^2 \rangle^{1/2} \cong 1.61$ mb. The nearness of mean and rms errors may indicate the fact that using a better temperature interpolation in the troposphere above the ocean surface will make it possible to reduce the error of determination of water vapor surface pressure significantly.

Conclusions.

The GPS together with planned LEO satellites provide an opportunity to create a space radio occultation system for obtaining continuous global fields of temperature, pressure and humidity with a spatial density substantially exceeding the existing radio sounding network. The characteristic property of radio occultation sounding as compared to the passive thermal sounding from satellites is the higher vertical resolution (about 0.5 km at GPS frequencies) and the direct retrieval of meteorological quantities as a function of altitude. The main results of our computational simulations of radio occultation sensing on the basis of the T106 model, aimed at accuracy estimations of the retrieval algorithms, are as follows:

1) The horizontal resolution (the characteristic horizontal smoothing scale for retrieved values of meteorological parameters), which is about 600 km in the case of independent data retrieval from single occultations by Abelian inversion, may be substantially improved by concurrently using data from different viewing directions in the retrieval algorithms (refraction tomography). For achieving T106-model resolution it is sufficient to use a sounding scheme with 3 viewing directions.

2) The accuracy of temperature and geopotential retrieval in the stratosphere (for the pressure

interval 200-20mb) is about 1K and 10 m, respectively, when an Abelian inversion is used and it is significantly improved to 0.01 K and 30 cm when using a tomographical iterative reconstruction based on a sounding scheme with 3 viewing directions.

3) Although the retrieval accuracy for refractivity is of the same size in the troposphere and stratosphere, the influence of humidity results in unacceptable errors in retrieved temperature and pressure below 5-7 km in middle latitudes and below 12-13 km in tropical regions. In tropical regions the error in surface temperature may reach 60-70 K indicating the possibility to determine humidity from RF refractivity by using idependently sounded tropospheric temperature data.

The computational simulation carried out was the first one testing the refractometric remote sensing of terrestrial atmosphere from space on the basis of GCM. The main result is that the problem of insufficient horizontal resolution, which seemed to be the main disadvantage of the method, may be apparently removed. However the measuring errors were not taken into consideration. Thus the obtained retrieval errors are only due to the approximate solution of the 3D inverse refraction problem in case of using the Abel inversion and due to discretization and incompleteness of measurements in case of tomographical reconstruction.

The very high accuracy required for ray tracing calculations resulted in a large computation time and did not allow to retrieve pressure and temperature fields for the whole globe in order to test their assimilation. For this purpose, the ray tracing programs have to be substantially developed to use the special advantages of vector processors.

It seems to be expedient to include the following problems for further consideration.

1) Modeling of measuring errors and including them in computations of the retrieval of atmospheric parameters from Doppler data.

2) Developing 3D retrieval programs for arbitrary orbital parameters of LEO satellites.

3) Using other data along with Doppler in retrieval algorithms (i.e. passive thermal sounding, radio sounding, etc.).

4) Using temperature data for deriving humidity from RF refractivity in troposphere (probably taking into account statistical characteristics of both temperature and humidity fields).

Acknowledgments

This work was sponsored by the Max-Planck-Society for the Advancements of Science. The authors would like to thank the staff of the Max-Planck Institute for Meteorology for the arrangement and general support of the investigation, in particular L.Bengtsson, E.Roeckner, B.Machenhauer, K.Arpe, J.Oberhuber for helpful discussions, and R.Budich for help in using the computer system.

References

Bean, B.R. and E.J.Datton, 1968: Radio Meteorology; *Dover Publ., Inc., New-York*, 7p.

Douglas, D.S., C.Goad, C.Morrison and F.Foster, 1980: Determination of Geopotential from Satellite-to-satellite Tracking Data; *J. of Geophys. Res.* **B10**, 5471-5480.

Eshleman, V.R., G.L.Tyler, J.D.Anderson, G.Fjeldbo, G.S.Levy, G.E.Wood and T.A.Croft, 1977: Radio Science Investigations with Voyager; *Space Sci. Rev.* **21**, 207-232.

Fishbach, F.F., 1965: A Satellite Method for Pressure and Temperature Below 24 km; *Bull. Amer. Meteor. Soc.* **9**, 528-532.

Fjeldbo, G. and V.R.Eshleman, 1968: The Atmosphere of Mars Analyzed by Integral Inversion of the Mariner IV Occultation Data; *Planet. Space Sci.* **16**, 123-140.

Gorbunov, M.E., 1988: Accuracy of the Refractometric Method in a Horizontally Nonuniform Atmosphere; *Izv., Atmosph. and Ocean. Phys.* **5**, 381-384.

Gorbunov, M.E., 1990: Solution of the Inverse Problems of Remote Atmospheric Refractometry on Limb Paths; *Izv., Atmosph. and Ocean. Phys.* **2**, 86-91.

Gorbunov, M.E. and A.S.Gurvich, (to appear): Remote Sensing of the Atmosphere Using a System of Synchronously Orbiting Satellites; *Radio Science.*

Gurvich, A.S. and S.V.Sokolovskiy, 1985: Reconstruction of a Pressure Field by Remote Refractometry from Space; *Izv., Atmosph. and Ocean. Phys.* **1**, 7-13.

Gurvich, A.S. and T.G.Krasilnikova, 1990: Navigation Satellites for Radio Sensing of the Earth's atmosphere; *Sov. J. of Remote Sensing* **6**, 1124-1130.

Gurvich, A.S., V.Kan, L.I.Popov, V.V.Ryumin, S.A.Savchenko and S.V.Sokolovskiy, 1982: Reconstruction of the Atmosphere's Temperature Profile from Motion Pictures of the Sun and Moon Taken from the "Salyut-6" Orbiter; *Izv., Atmosph. and Ocean. Phys.* **1**, 1-4.

Hardy, K.R., D.P.Hinson, G.L.Tyler and E.R.Krusinski, 1992: Atmospheric Profiles from Active Space-Based Radio Measurements; *Prepr. of the 6-th Conf. on Satellite Meteorology and Climatology* Jan.5-10, Atlanta, GA.

Lindal, G.F., et al., 1981: The Atmosphere of Jupiter: An Analysis of the Voyager Radio Occultation Measurements; *J. Geophys. Res.* **86**, 8721-8727.

Lusignan, B., G.Modrell, A.Morrison, J.Pomalaza and S.G.Ungar, 1969: Sensing the Earth's Atmosphere with Occultation Satellites; *Proc. of the IEEE* **4**, 458-467.

Natterer, F., 1986: *The Mathematics of Computerized Tomography*. B.G.Teubner, Stuttgart, John Wiley & Sons.

Parkinson, R.W. and S.W.Gilbert, 1983: Global Positioning System - Ten Years Later; *Proc. of the IEEE* **10**, 1177-1186.

Rangaswamy, S., 1976: Recovery of Atmospheric Parameters from the APOLLO/SOYUZ-ATS-F Radio Occultation Data; *Geophys. Res. Lett.* **8**, 483-486.

Roeckner, E., K.Arpe, L.Bengtsson, S.Brinkop, L.Dümenil, M.Esch, E.Kirk, F.Lunkeit, M.Ponater, B.Rockel, R.Sausen, U.Schlese, S.Schubert and M.Windelband, 1992: Simulation of the Present-Day Climate with the ECHAM Model: Impact of Model Physics and Resolution; *Report No.93, Max-Planck-Institute for Meteorology*.

Sokolovskiy, S.V., 1990: Solution of the Inverse Refraction Problem by Sensing of the Atmosphere from Space; *Sov. J. of Remote Sensing* **3**, 333-338.

Deutsches Klimarechenzentrum (DKRZ), 1992: The ECHAM3 Atmospheric General Circulation Model; *DKRZ Technical Report No.6*, edited by Modellbetreuungsgruppe (DKRZ).

Volkov, A.A., G.M.Grechko, A.S.Gurvich, V.Kan and S.V.Sokolovskiy, 1987: Recovery of the Vertical Temperature Profile of the Atmosphere from Refraction Measurements Made from the "Salyut-7" Station; *Izv., Atmosph. and Ocean. Phys.* **11**, 914-915.

Ware, R., 1992: GPS Sounding of the Earth's Atmosphere; *GPS World* September, 56-57.

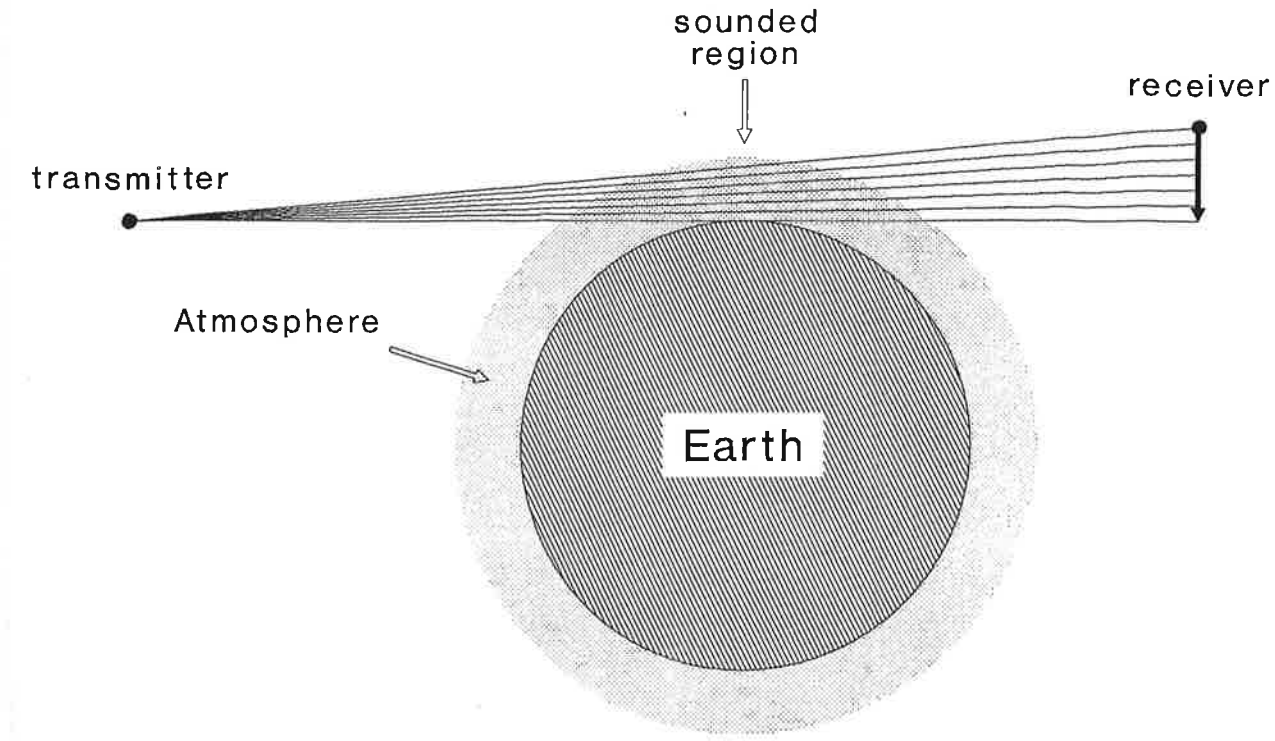

Fig. 1: Lay-out of refraction measurements during occultation from space. While receiver is moving in the field of electromagnetic wave refracted in the atmosphere, either angular (in optical domain) or Doppler (in radio frequency domain) data can be measured. The vertical profile of refractivity in the sounded region is to be retrieved.

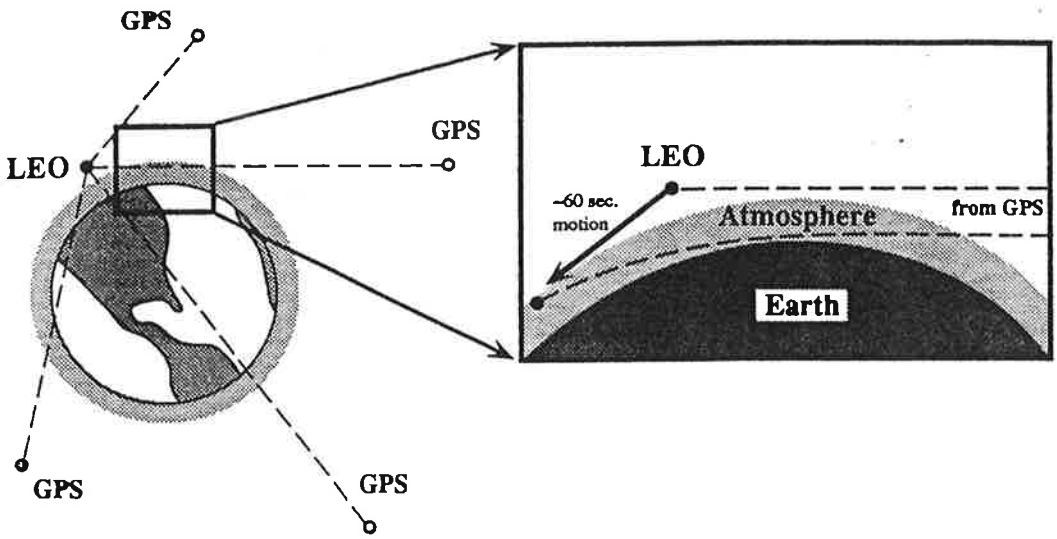

Fig. 2: A scheme of the GPS occultation concept (after Hardy et al. 1992).

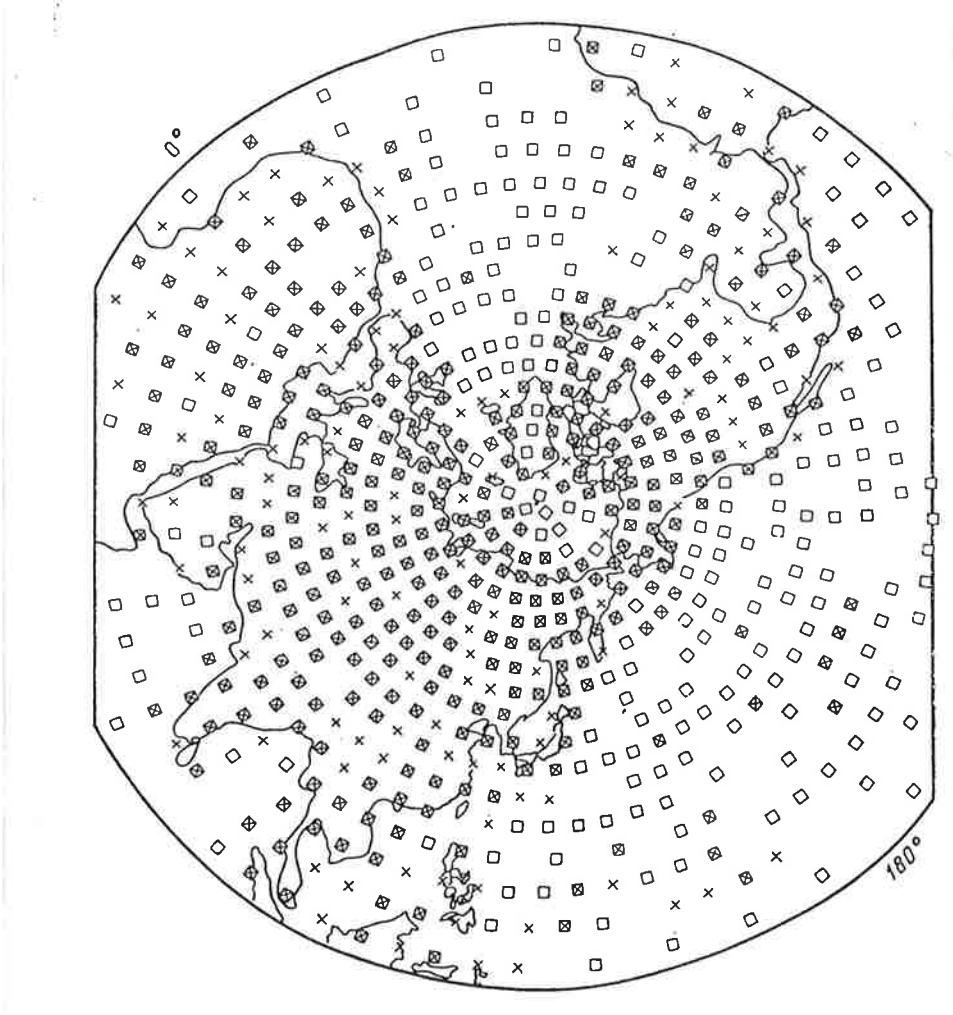

Fig. 3: The network of refractometric soundings in the northern hemisphere during 24 hours using 18 GPS satellites and 4 additional satellites at altitudes 870 km (after Gurvich and Krasilnikova 1990). □ refractometric soundings, × radiosondes.

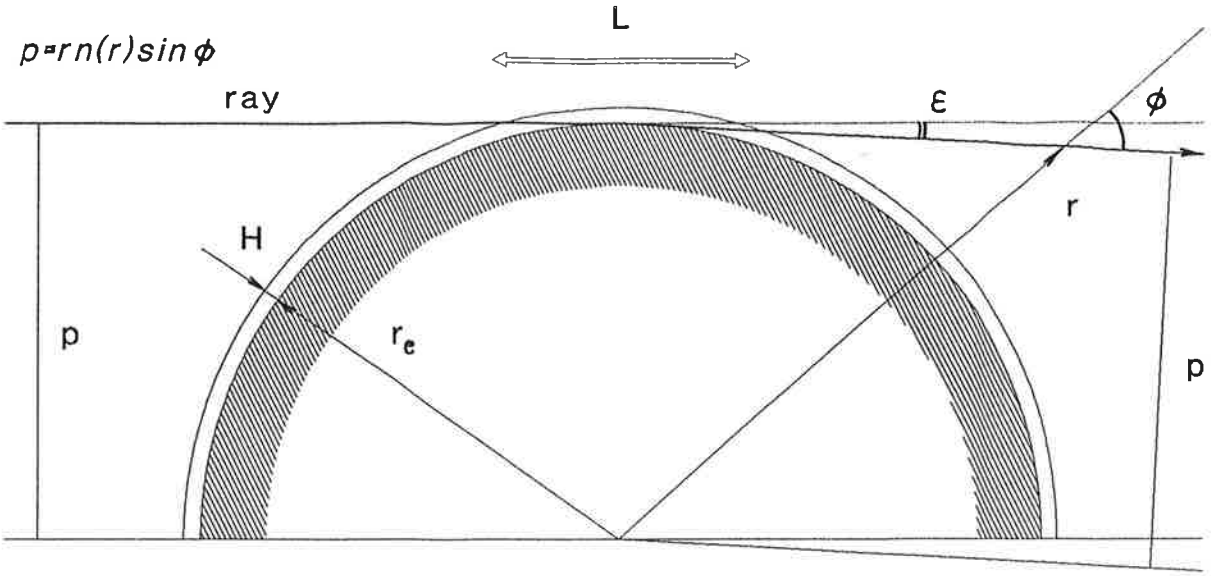

Fig. 4: Approximation of local spherically-symmetric distribution of refractivity. $L \cong 2\,(2r_e H)^{1/2}$ is the characteristic length of interaction between an electromagnetic wave and atmosphere.

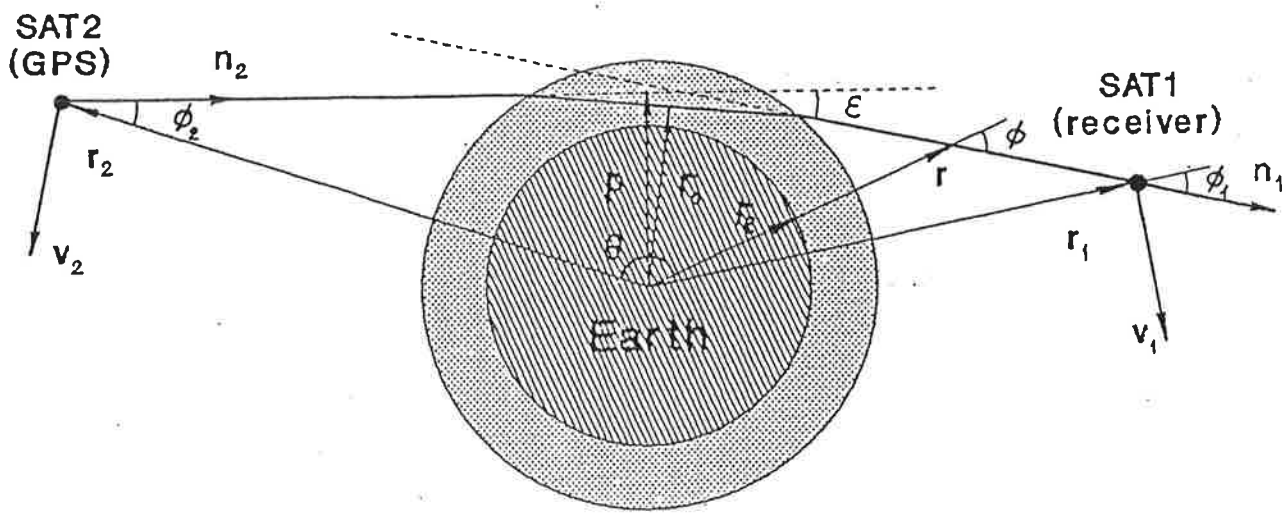

Fig. 5: Lay-out of refracted electromagnetic ray with notations.

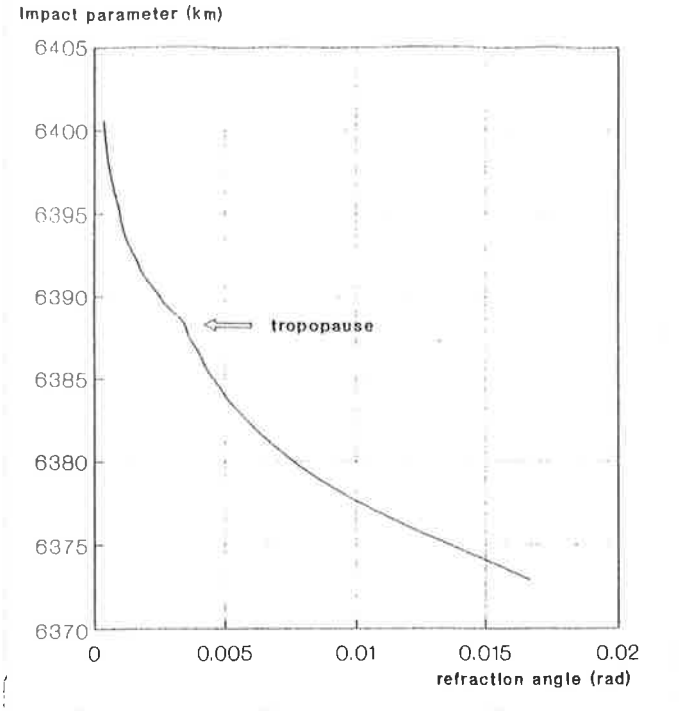

Fig. 6a: An example of the refraction angle as a function of the impact parameter of the ray calculated on the basis of the T106 model.

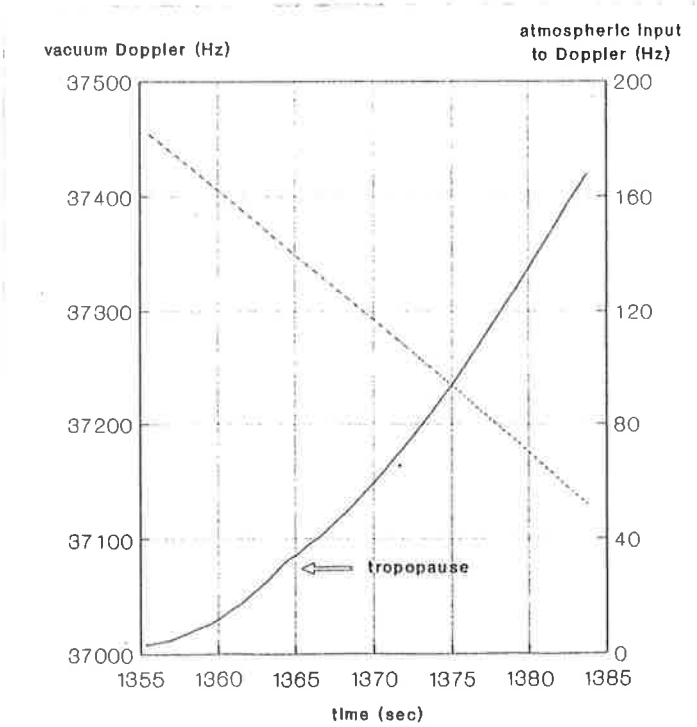

Fig. 6b: An example of the Doppler shift as a function of time for the frequency 1.5 Ghz and LEO height 250 km. Dashed line - full Doppler in vaccum; solid line - atmospheric input into Doppler calculated on the basis of the T106 model.

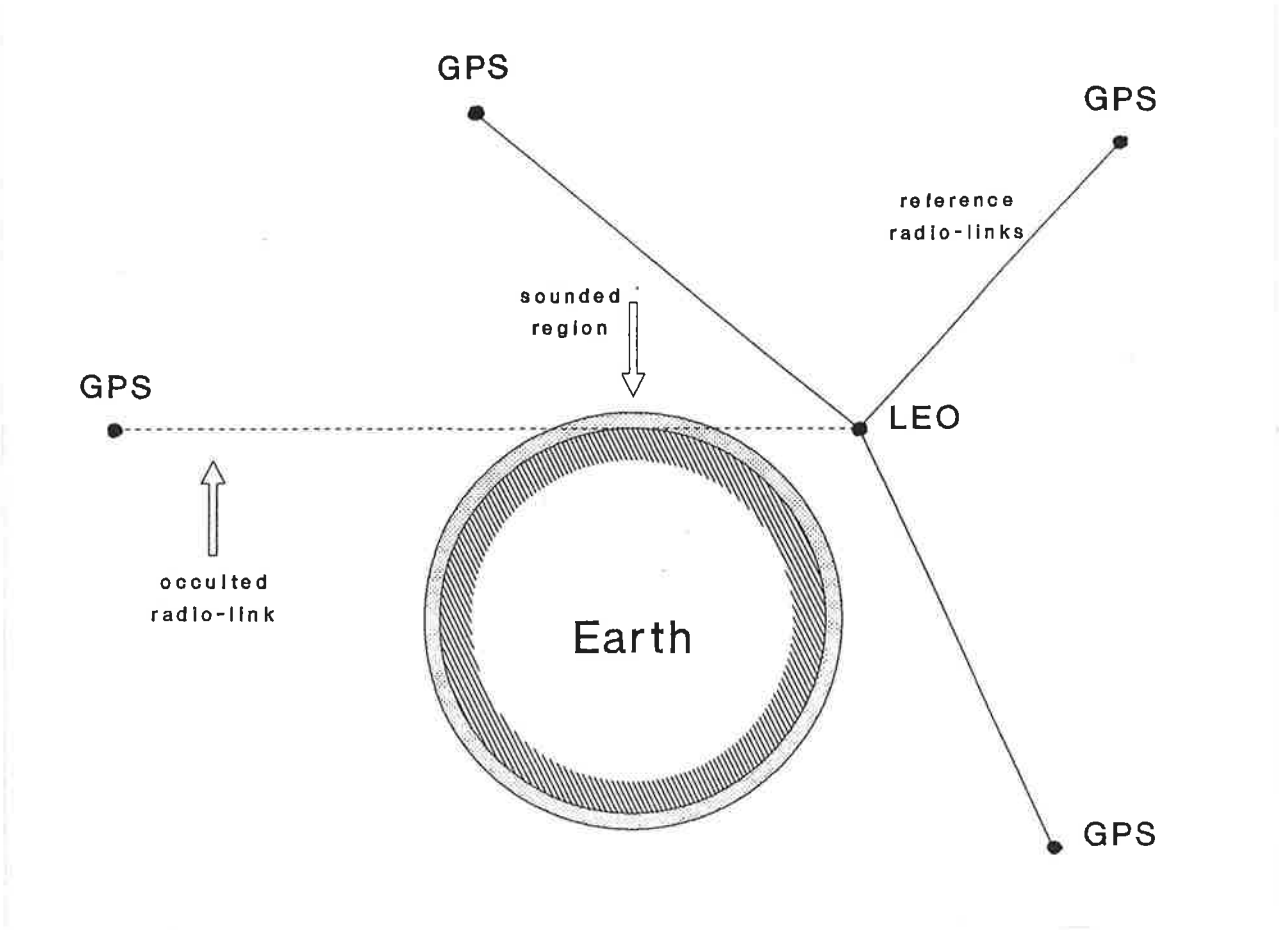

Fig. 7: Lay-out of radio occultation atmospheric sounding with 4 GPS satellites and 1 LEO satellite.

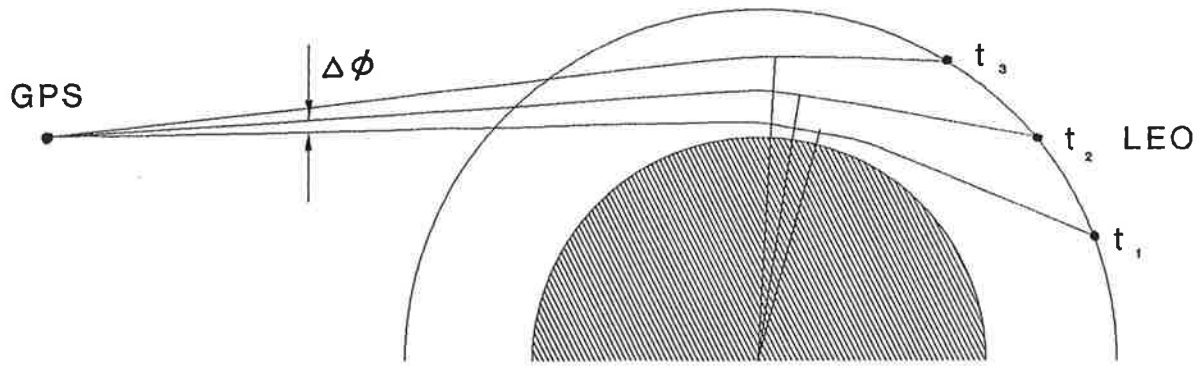

Fig. 8: Calculation of the bundle of rays in the LEO plain without using shooting methods.

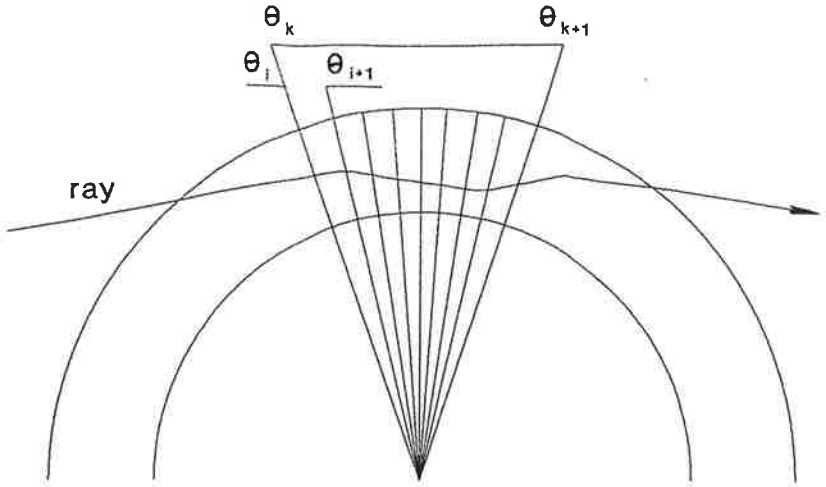

Fig. 9: The grid for horizontal interpolation of refractivity in the plain of low-earth-orbit (LEO).

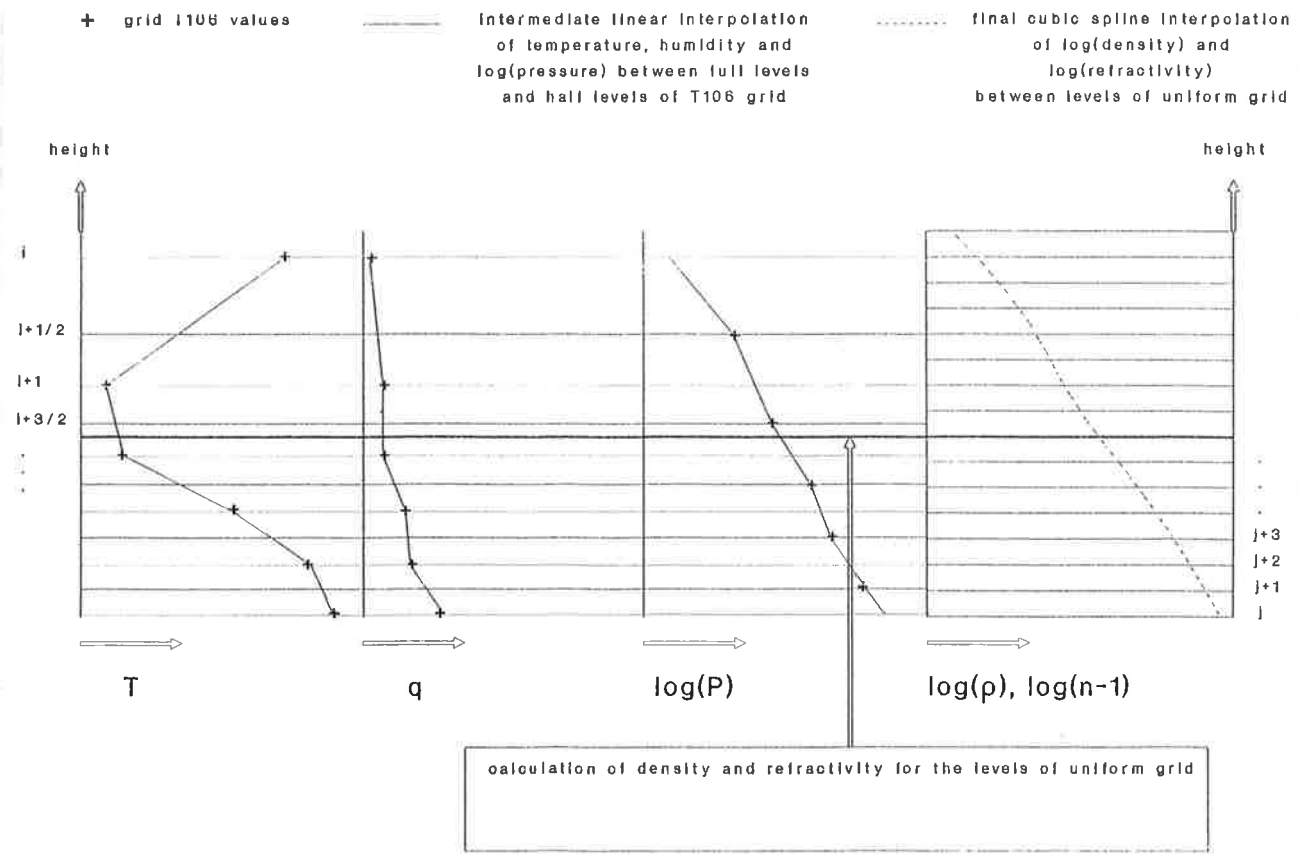

Fig. 10: The scheme of vertical interpolation of density and refractivity for T106 model.

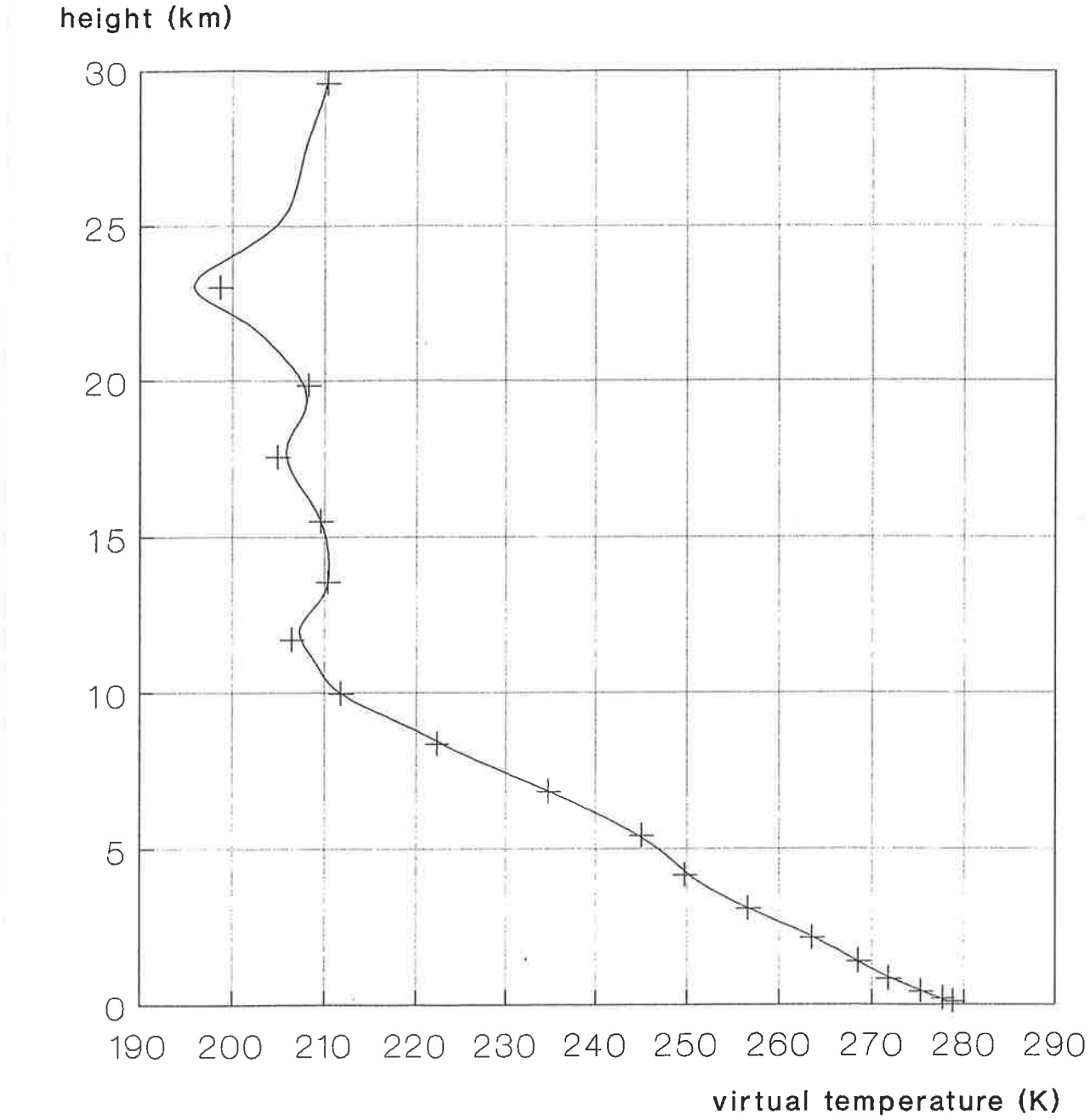

Fig. 11: An example of the vertical profile of virtual temperature T_v derived from continuously interpolated density and comparison with T106 grid values.

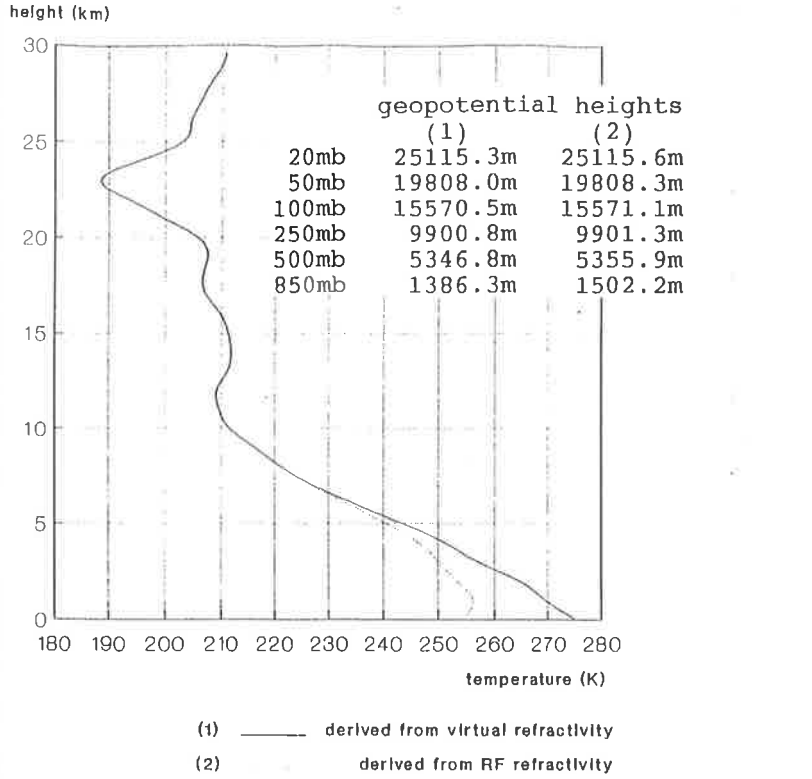

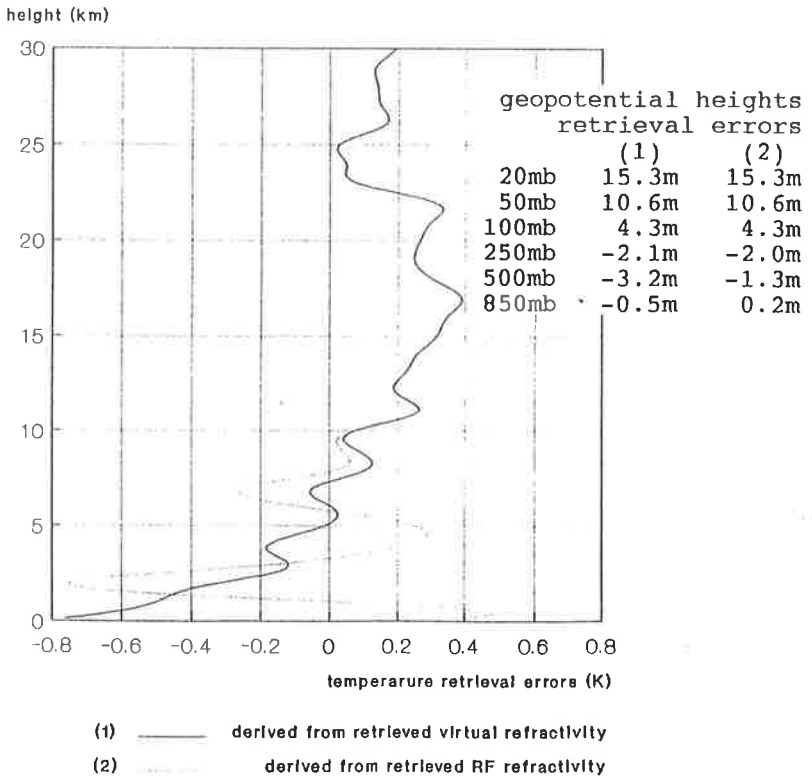

Fig. 12: The results of temperature and geopotential retrieval on the basis of the T106 model. Grid point (33,10) latitude +53.27°, longitude +10.125° (Hamburg).

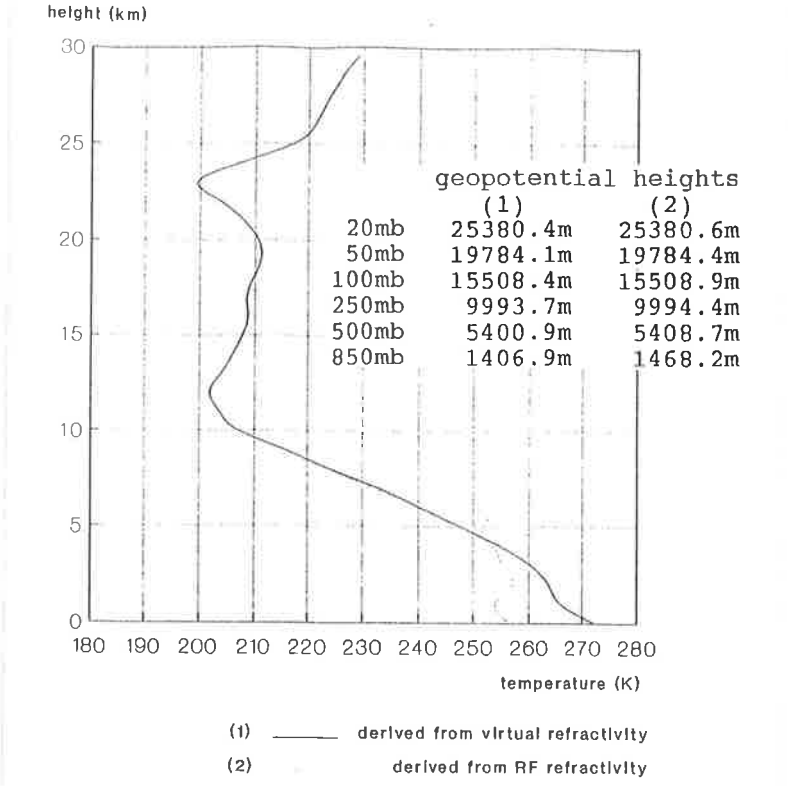

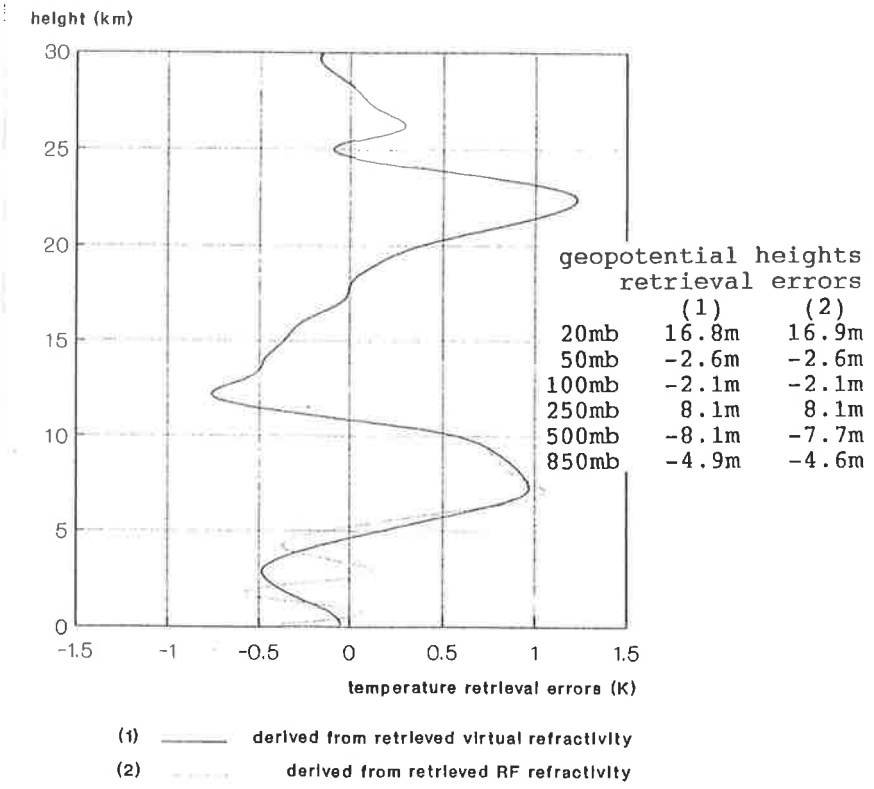

Fig. 13: The results of temperature and geopotential retrieval on the basis of the T106 model. Grid point (31,34) latitude +55.513°, longitude +37.125° (Moscow).

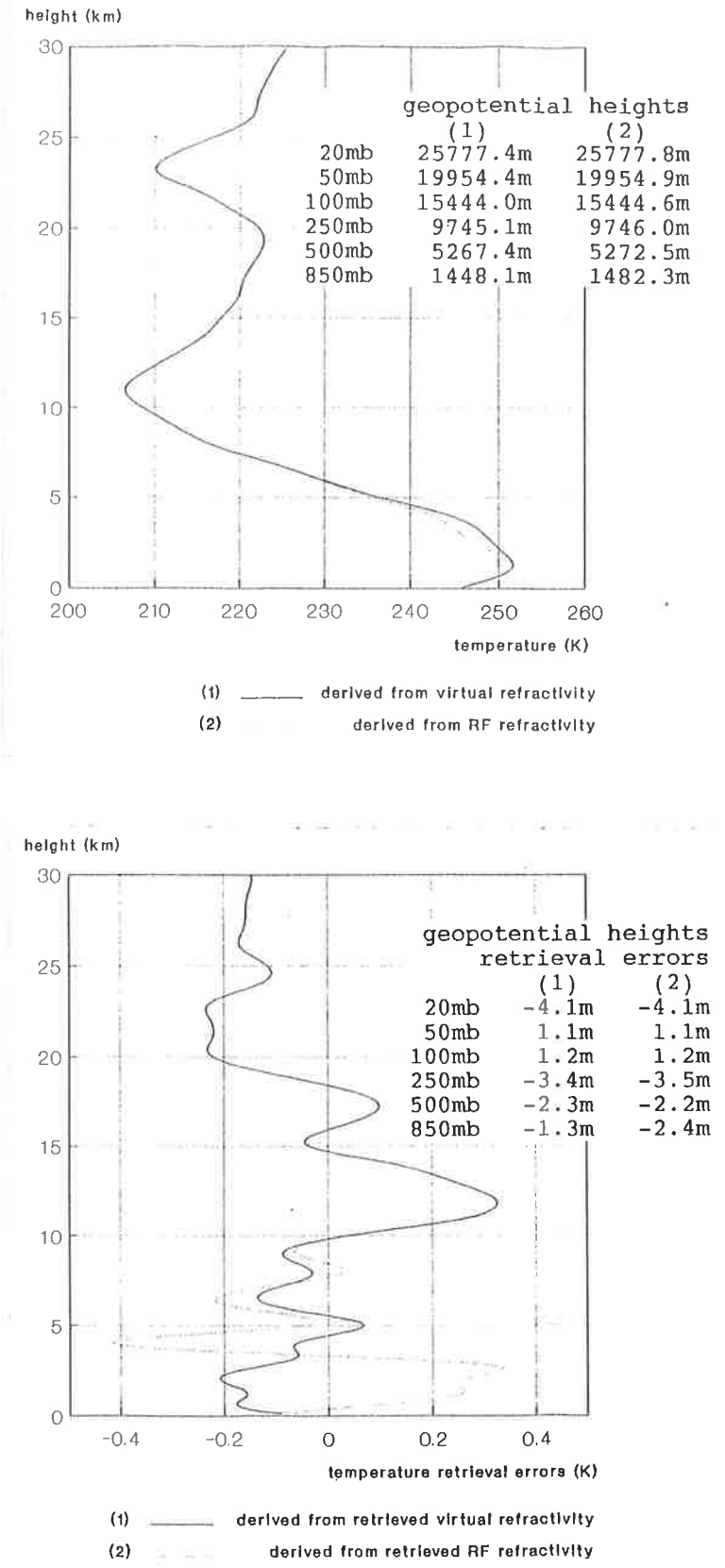

Fig. 14: The results of temperature and geopotential retrieval on the basis of the T106 model. Grid point (1,1) latitude +89.141°, longitude 0° (the North Pole).

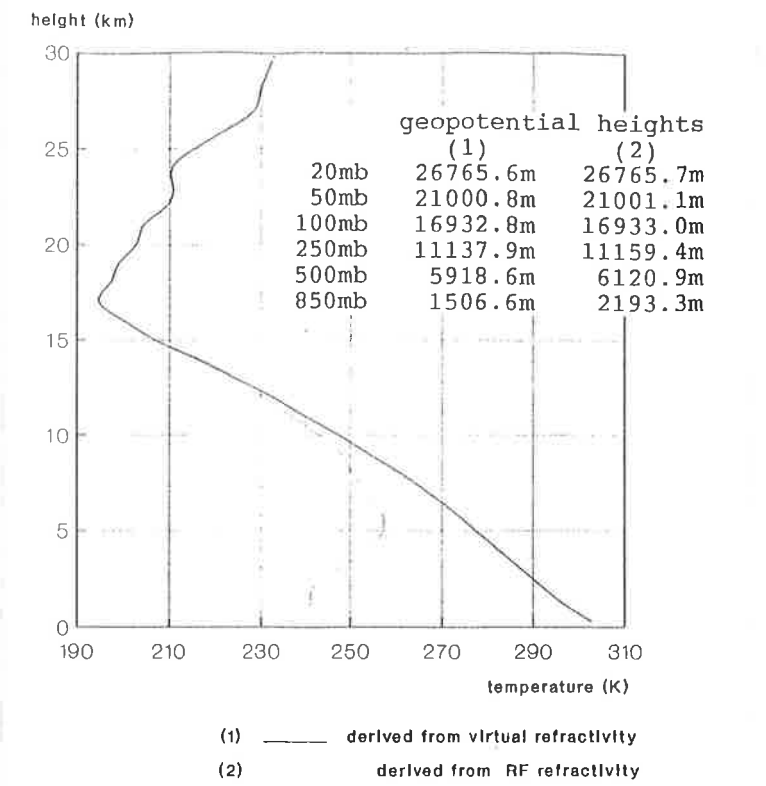

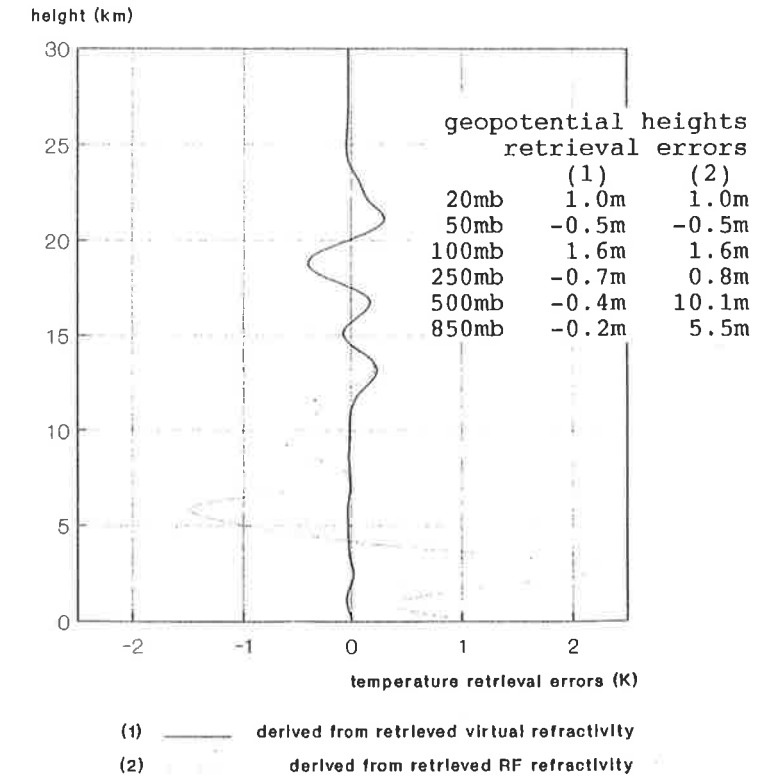

Fig. 15: The results of temperature and geopotential retrieval on the basis of the T106 model. Grid point (80,160) latitude +0.56°, longitude +178.875° (the center of the Pacific Ocean).

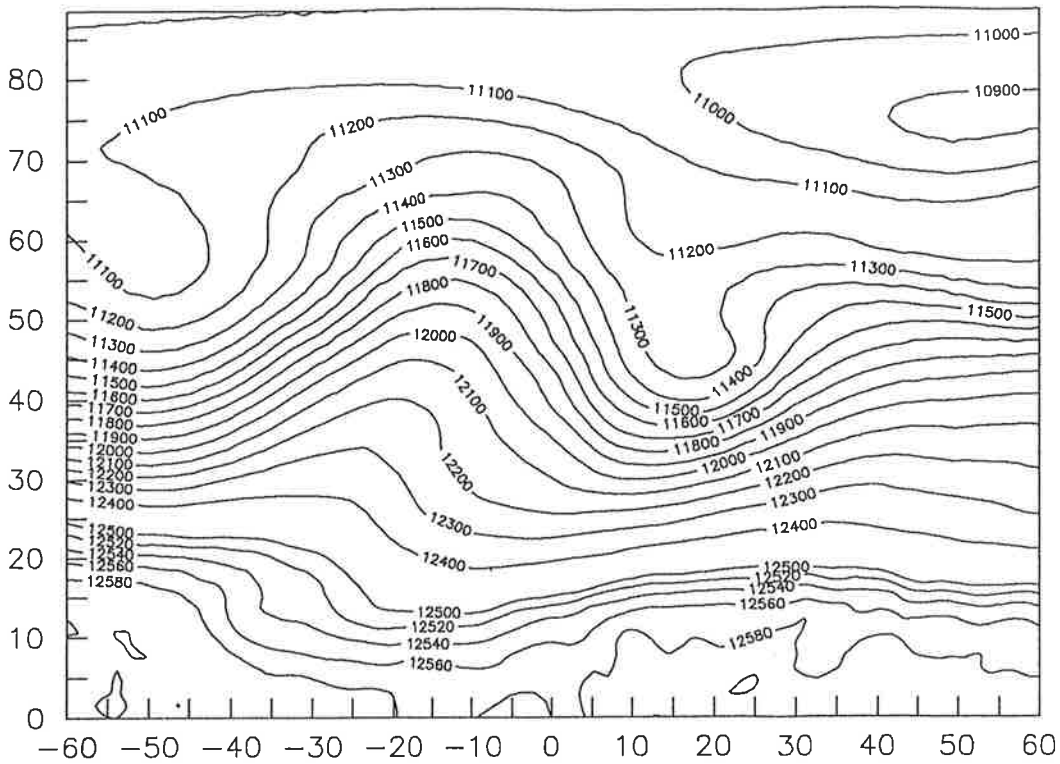

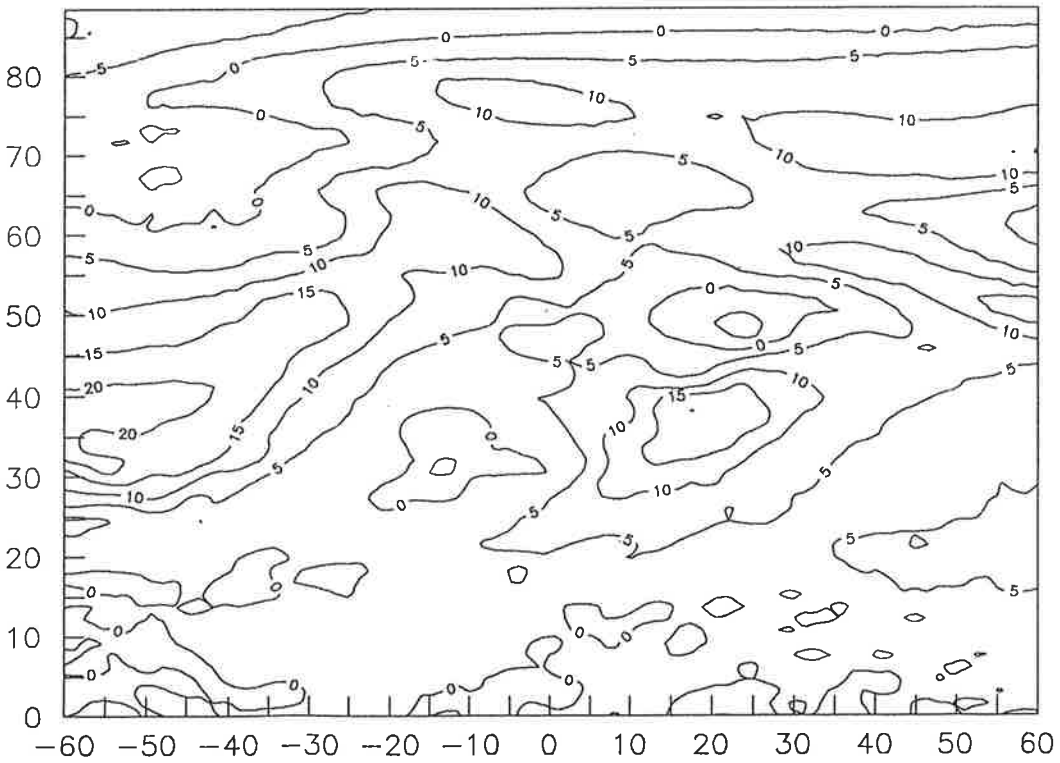

Fig. 16: Retrieval of 200 mb geopotential by Abellian inversion (0°-90° latitude, -60°÷60° longitude).

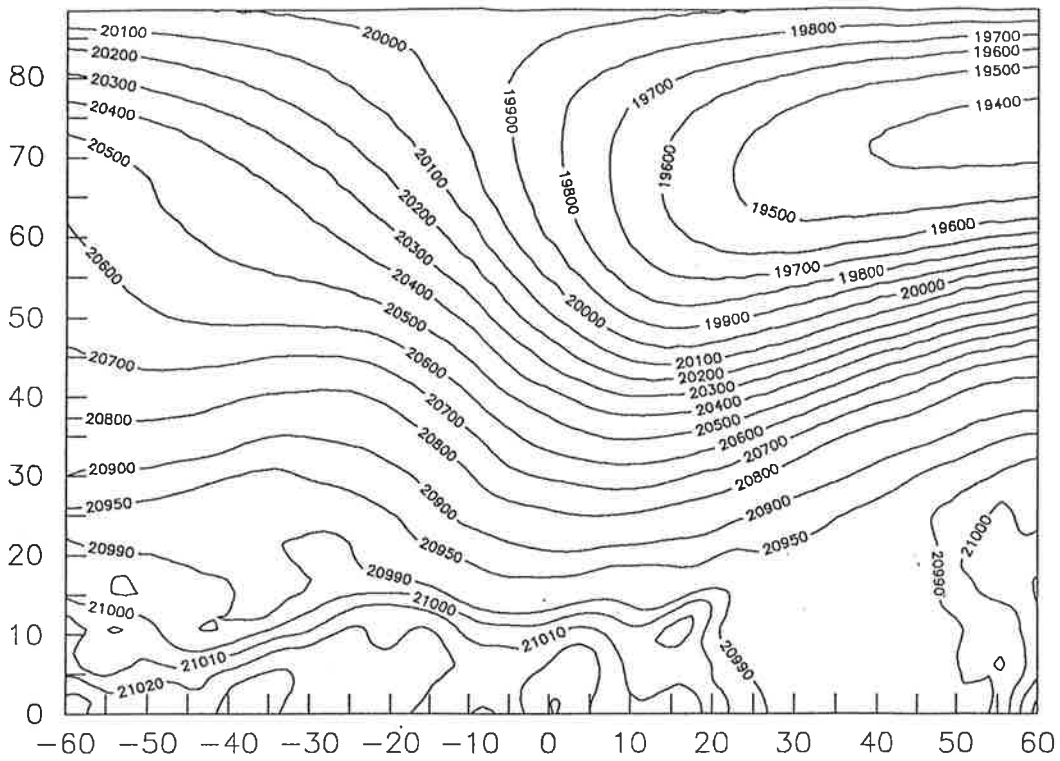

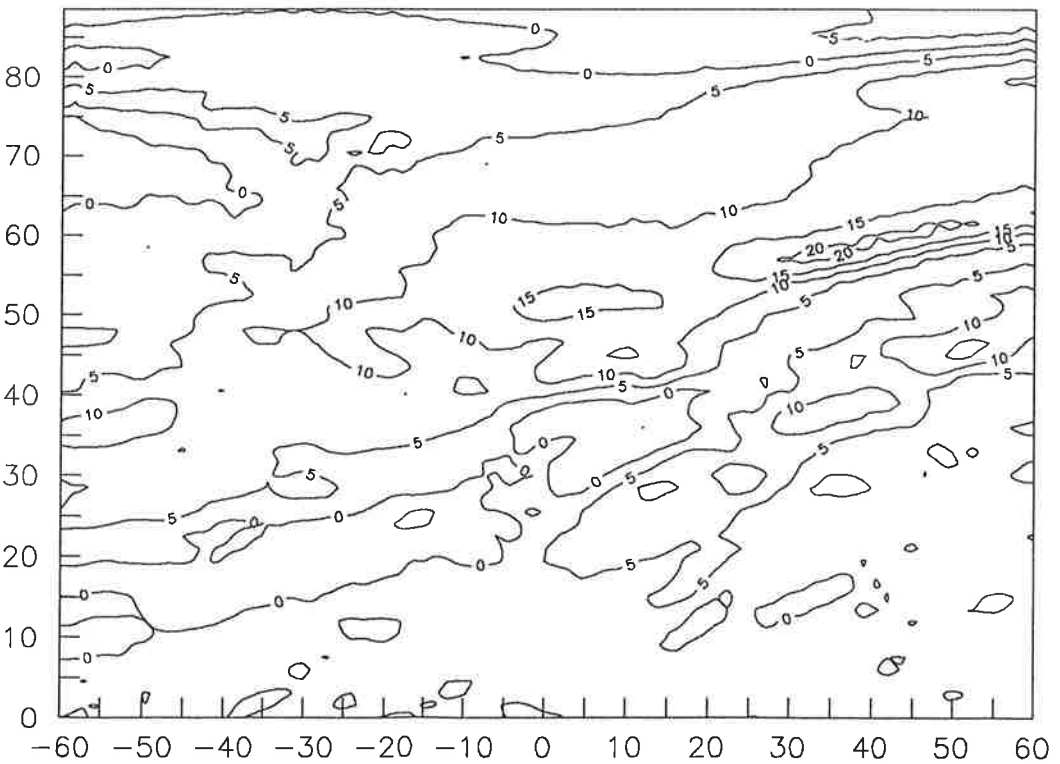

Fig. 17: Retrieval of 50 mb geopotential by Abellian inversion (0°-90° latitude, -60°÷60° longitude).

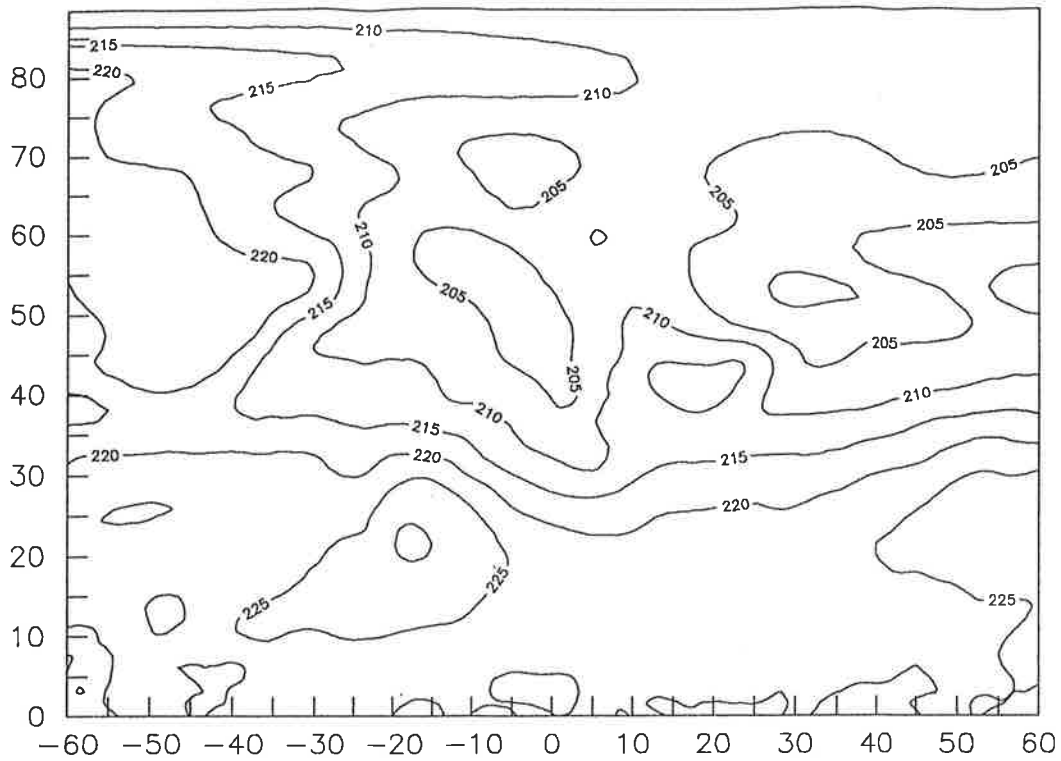

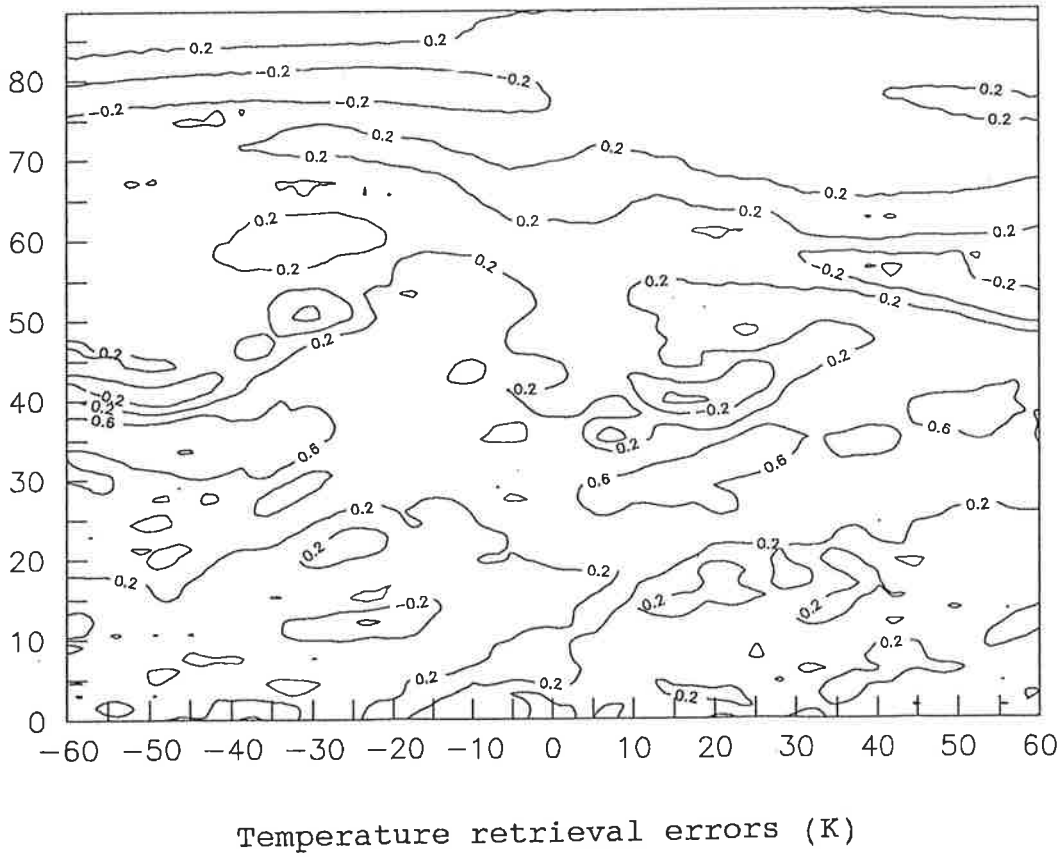

Fig. 18: Retrieval of 200 mb temperature by Abellian inversion (0°-90° latitude, -60°+60° longitude).

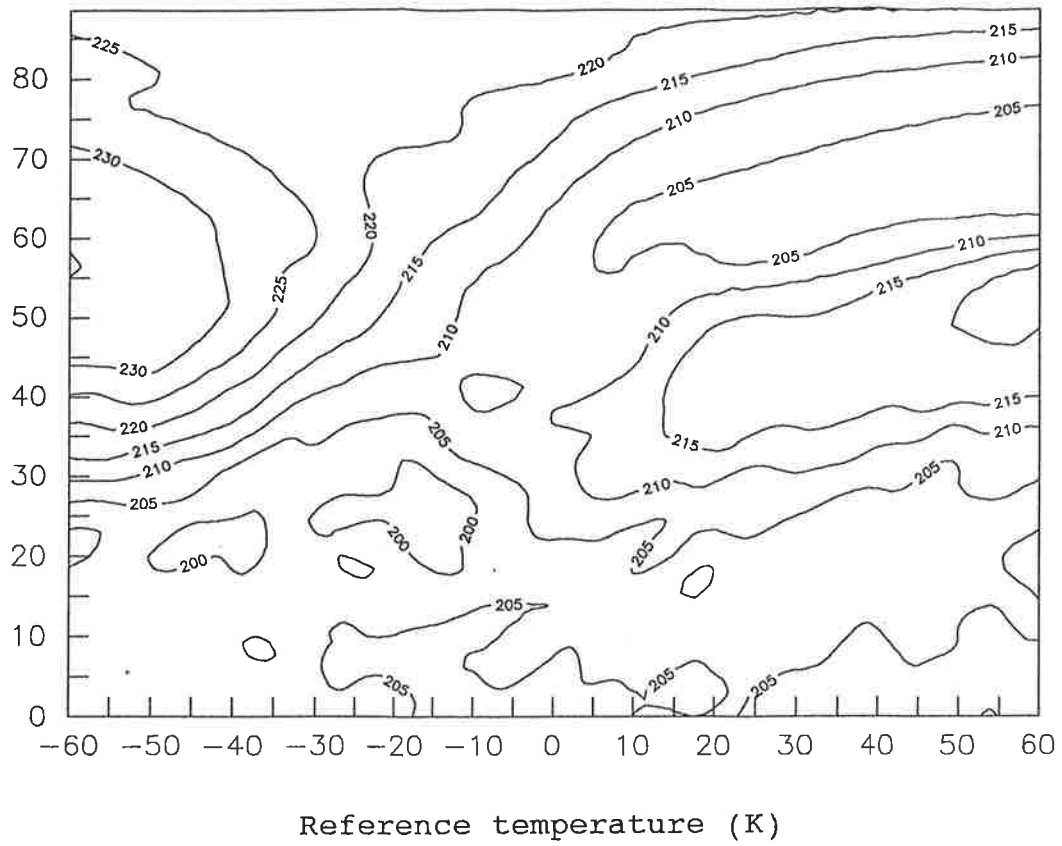

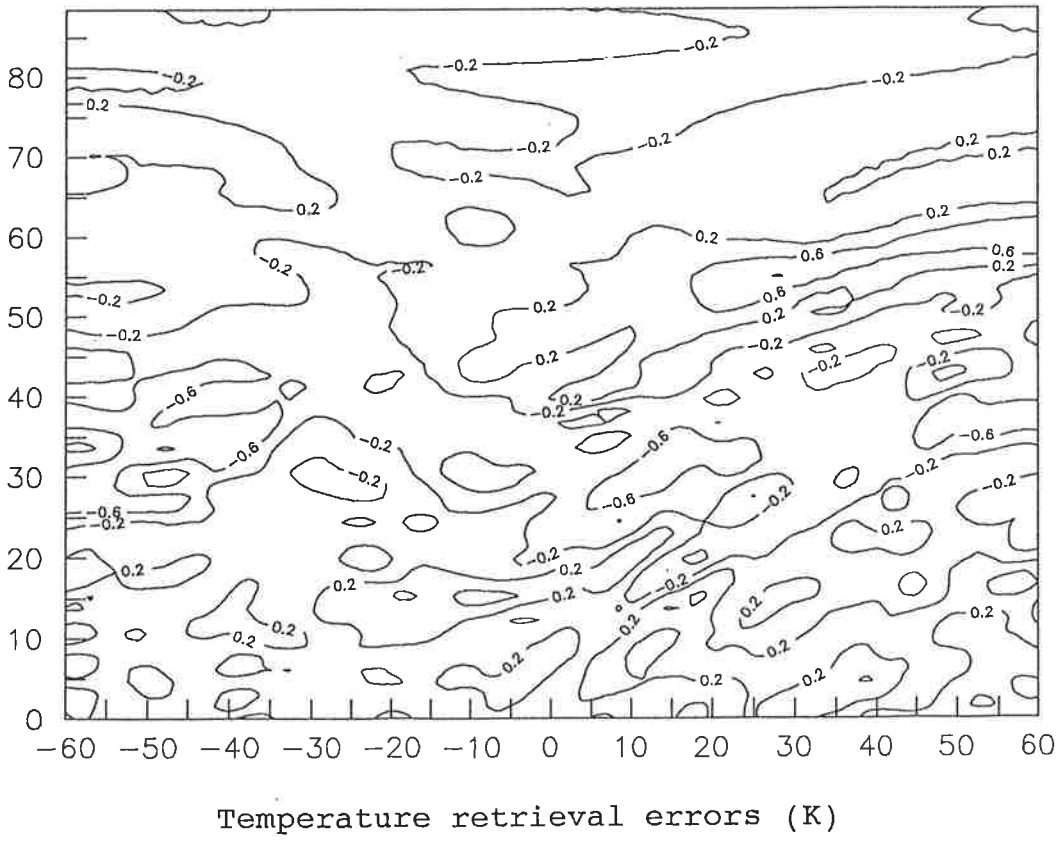

Fig. 19: Retrieval of 50 mb temperature by Abellian inversion (0°-90° latitude, -60°÷60° longitude).

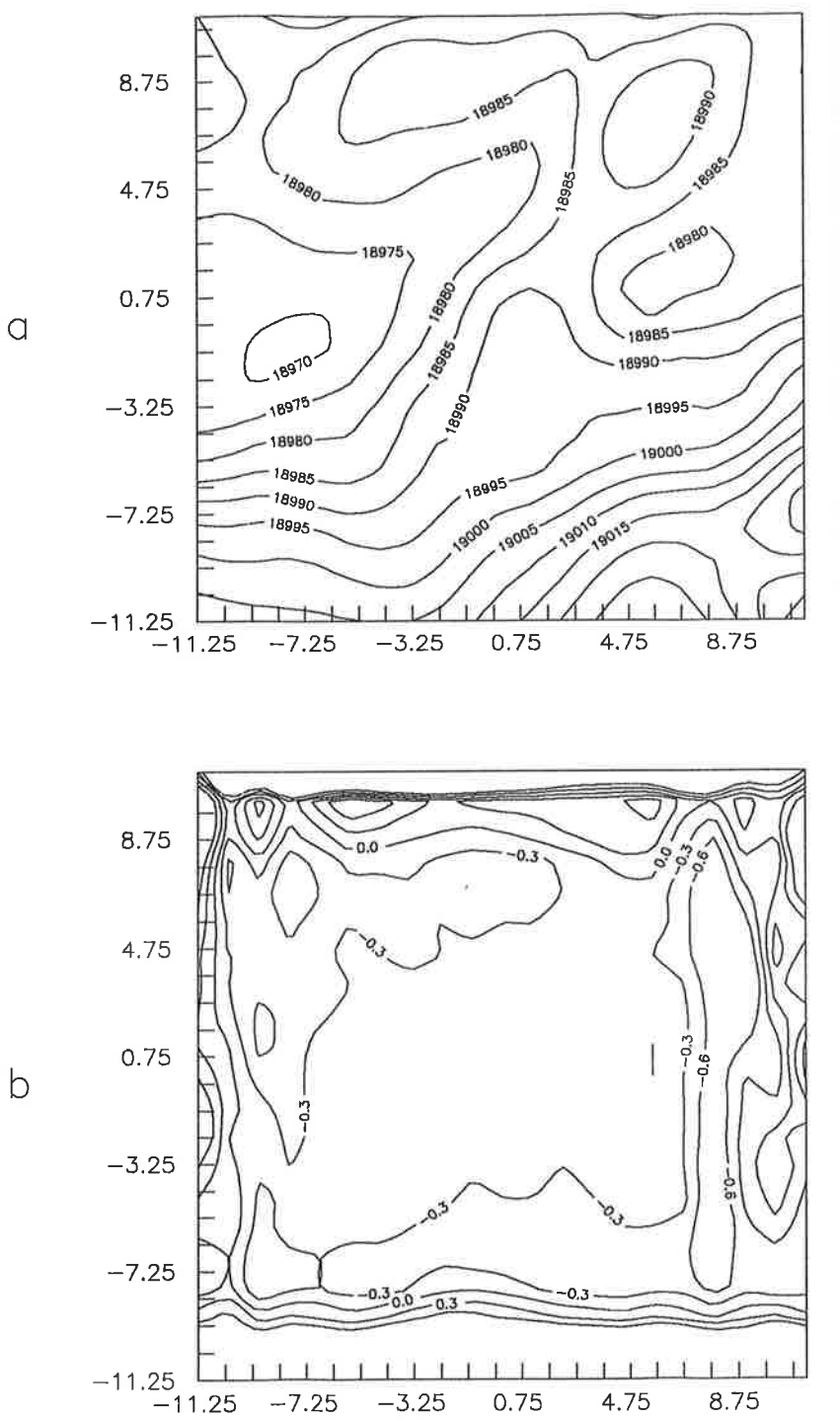

Fig. 20: Equatorial region: initial geopotential (a) and its errors (b) for 70 mb pressure level.

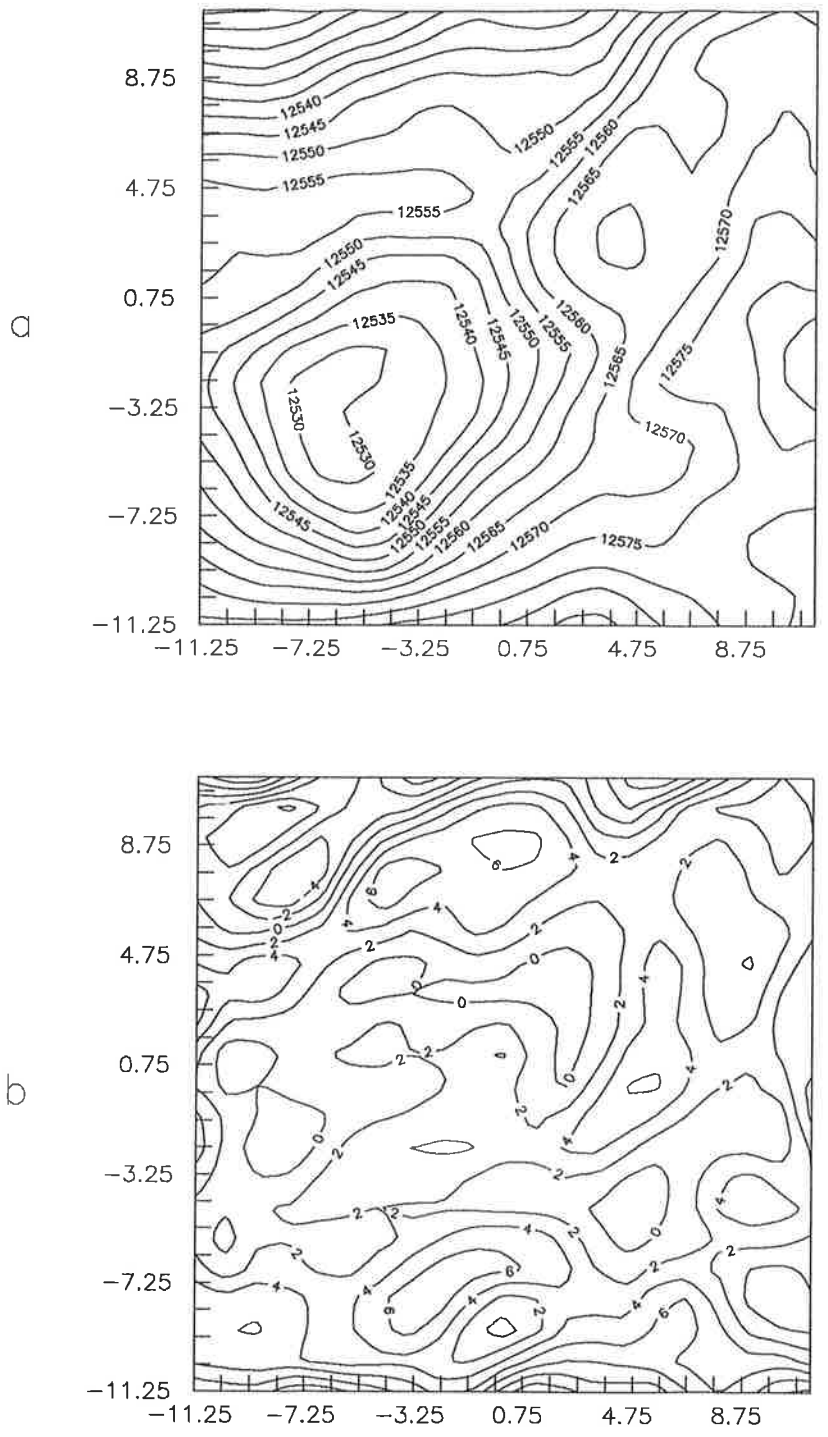

Fig. 21: Equatorial region: initial geopotential (a) and its errors (b) for 200 mb pressure level.

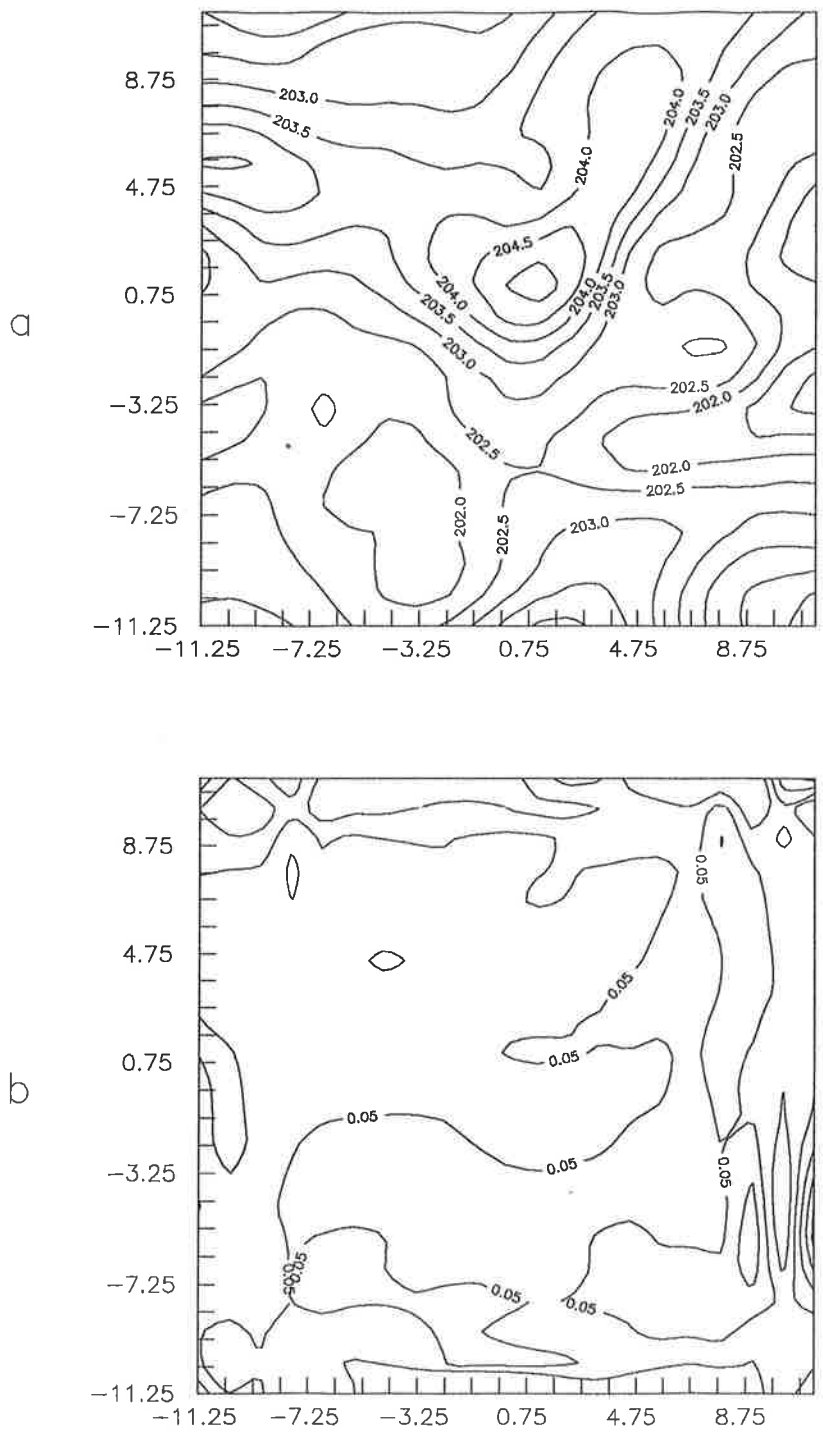

Fig. 22: Equatorial region: initial temperature (a) and its errors (b) for 70 mb pressure level.

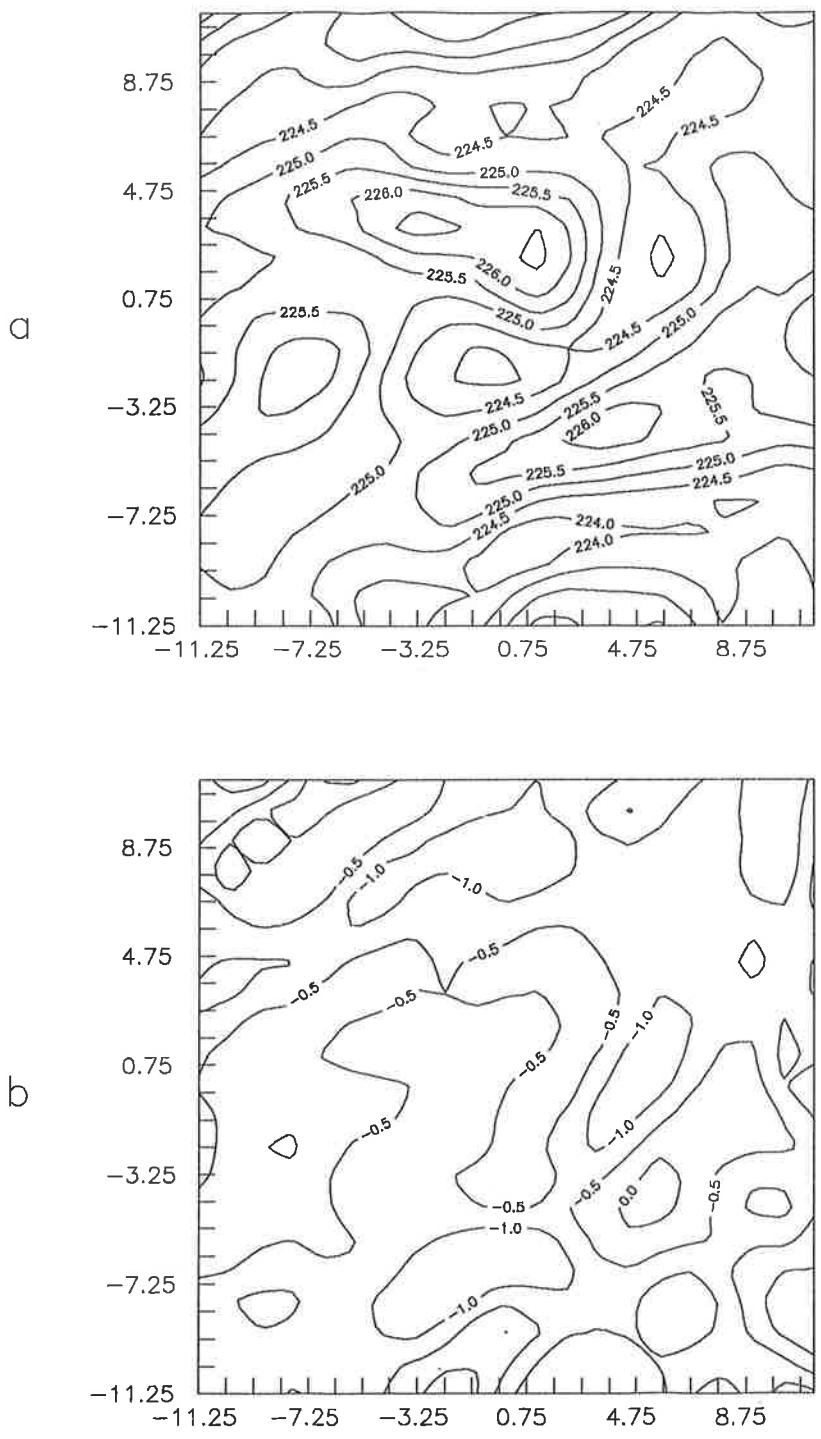

Fig. 23: Equatorial region: initial temperature (a) and its errors (b) for 200 mb pressure level.

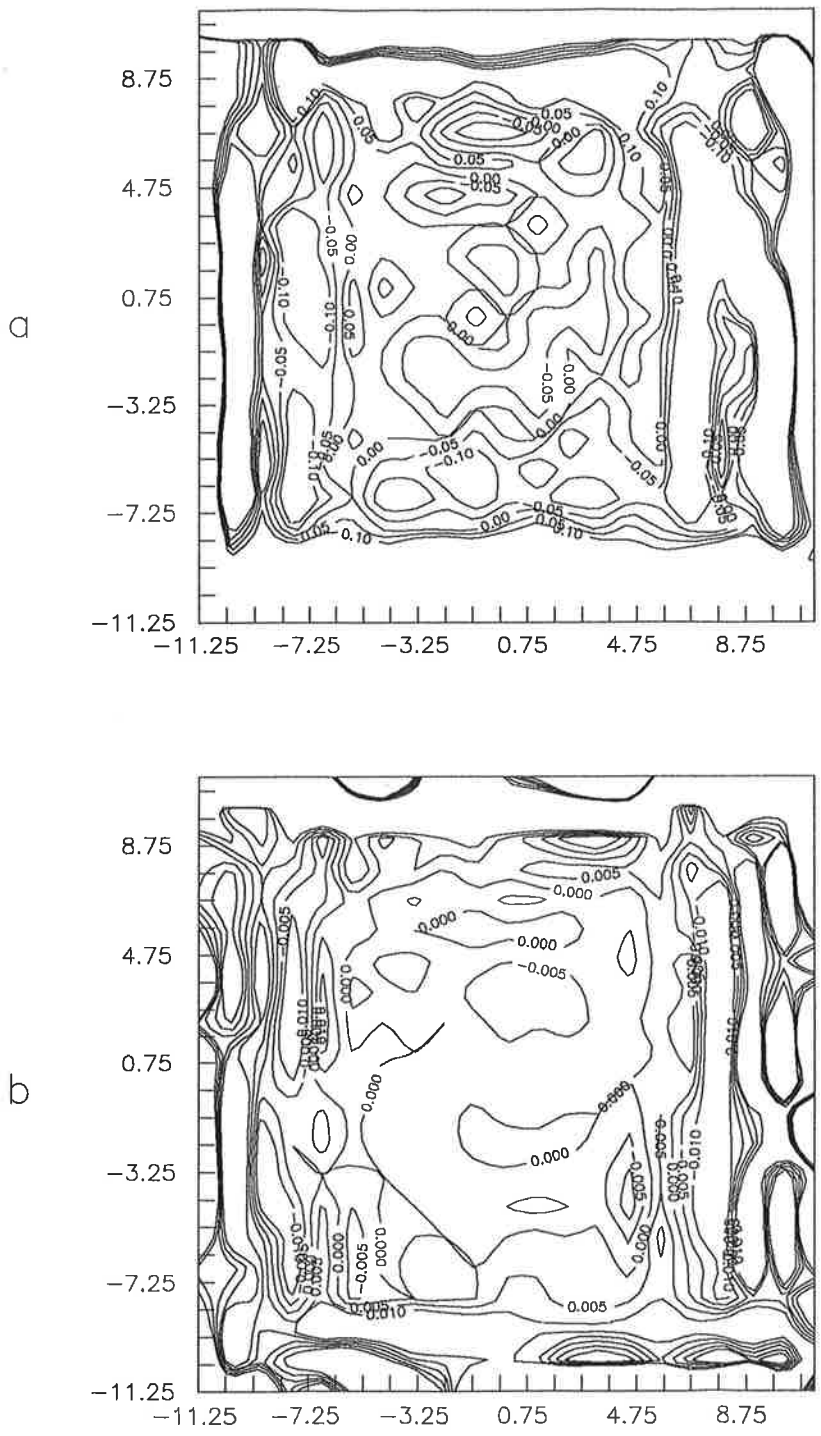

Fig. 24: Equatorial region: dry geopotential error (a) and dry temperature error (b) for 200 mb pressure level.

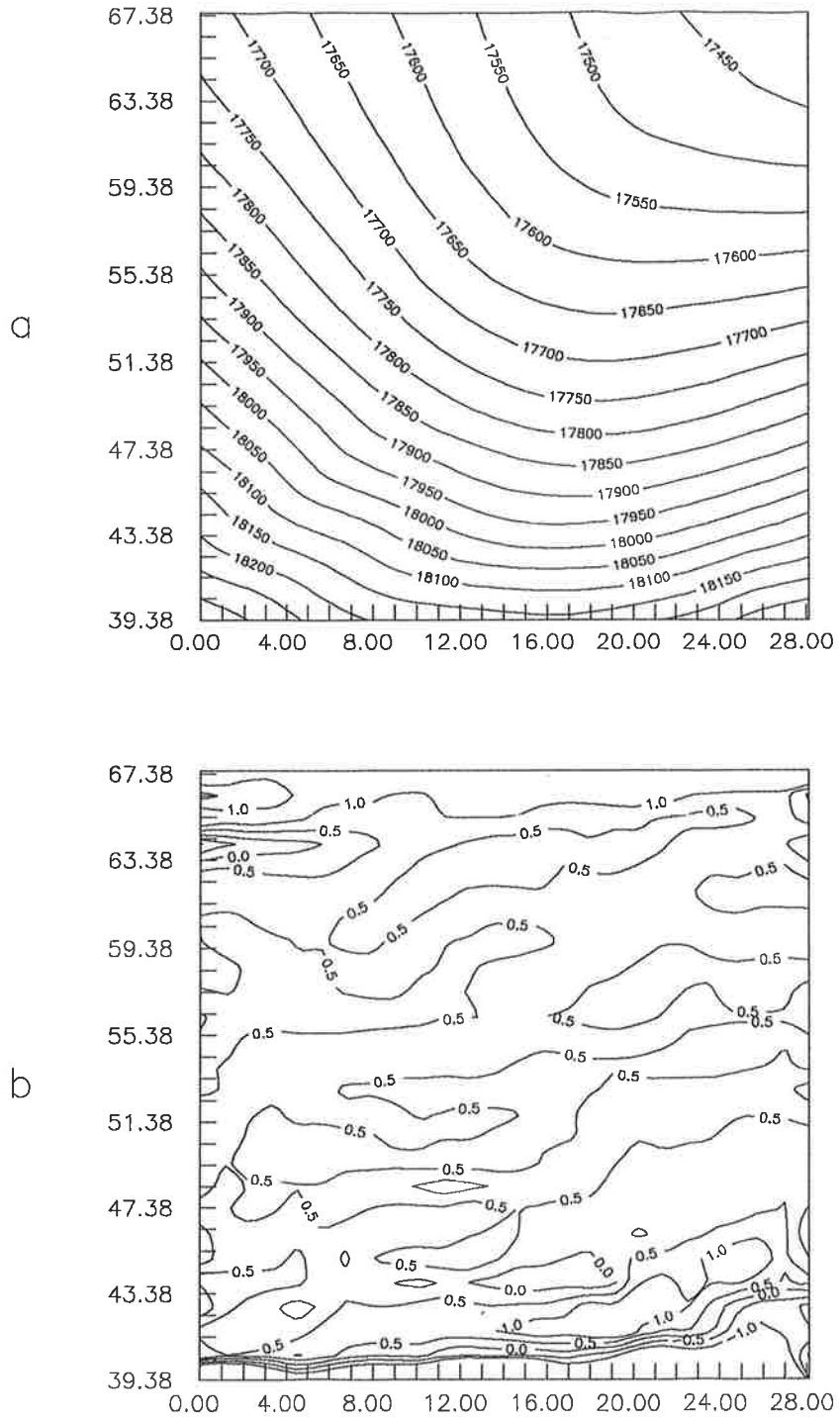

Fig. 25: European region: initial geopotential (a) and its errors (b) for 70 mb pressure level.

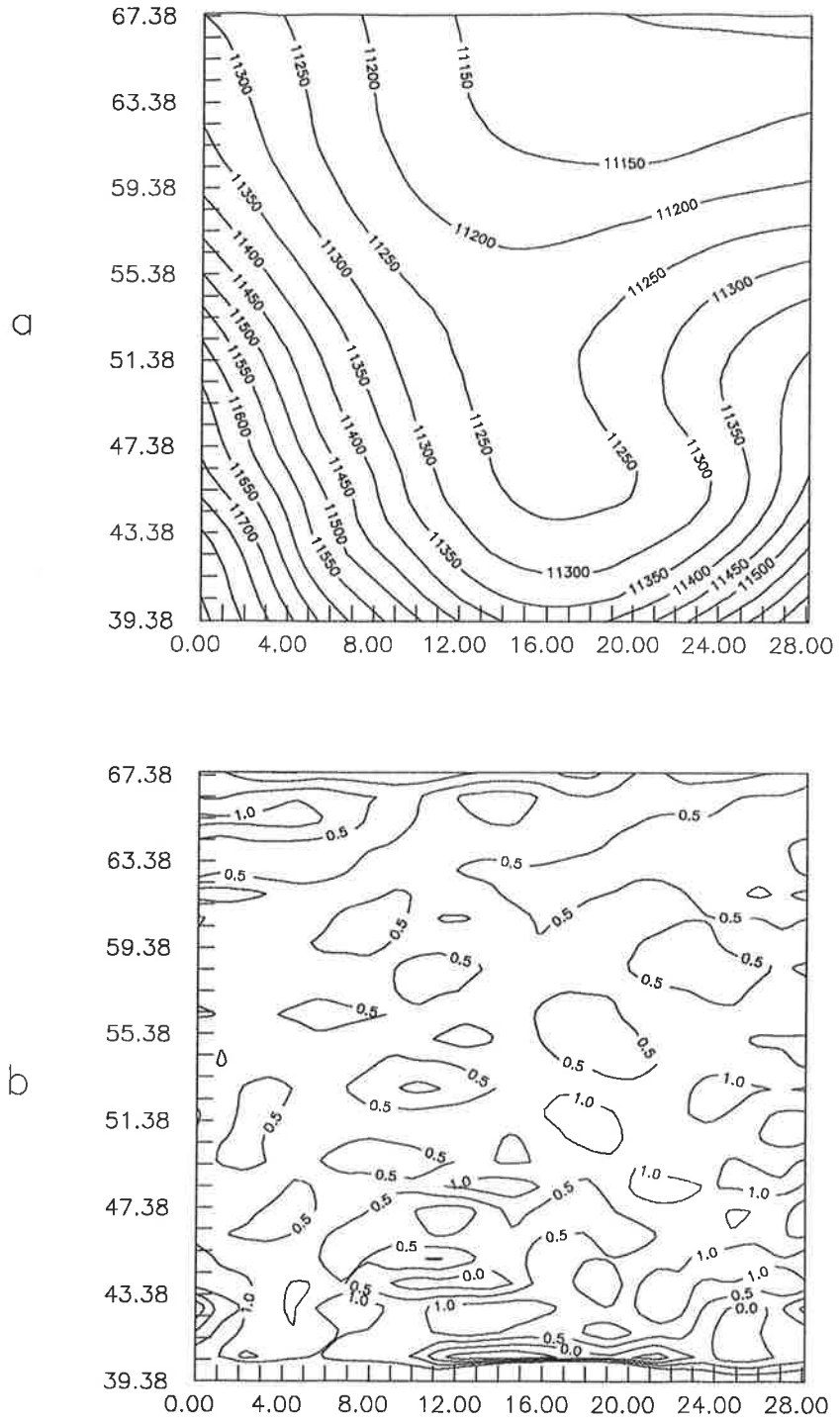

Fig. 26: European region: initial geopotential (a) and its errors (b) for 200 mb pressure level.

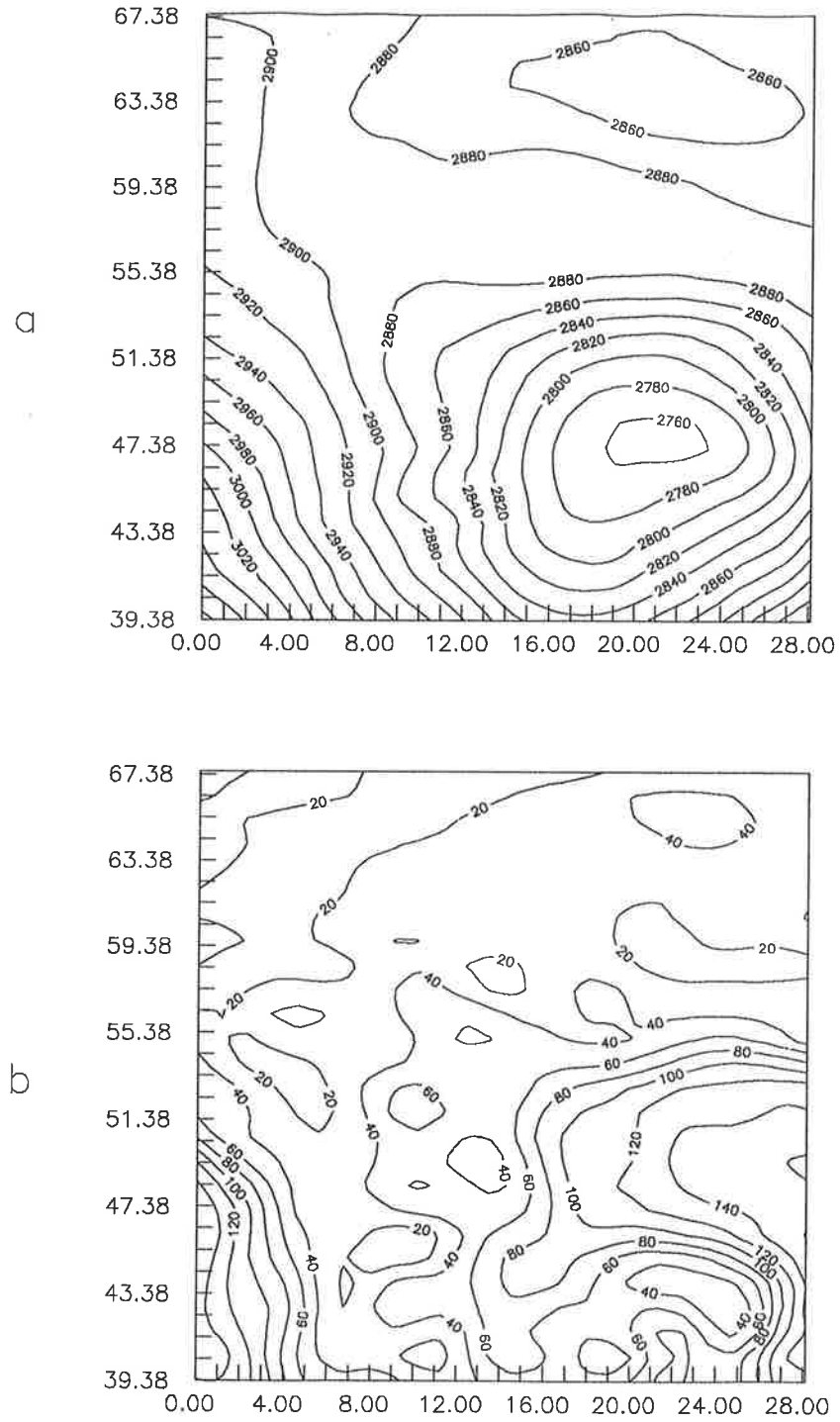

Fig. 27: European region: initial geopotential (a) and its errors (b) for 700 mb pressure level.

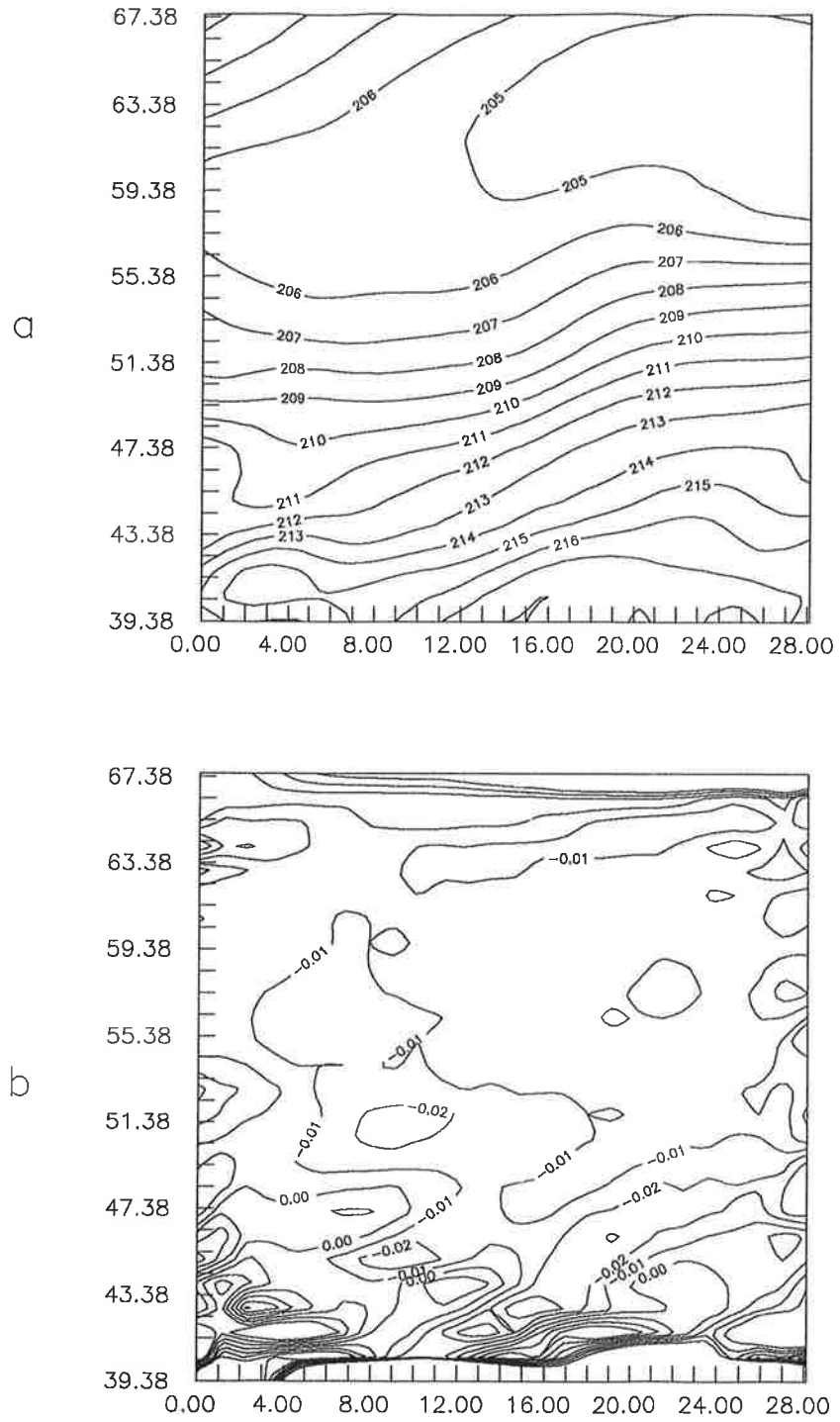

Fig. 28: European region: initial temperature (a) and its errors (b) for 70 mb pressure level.

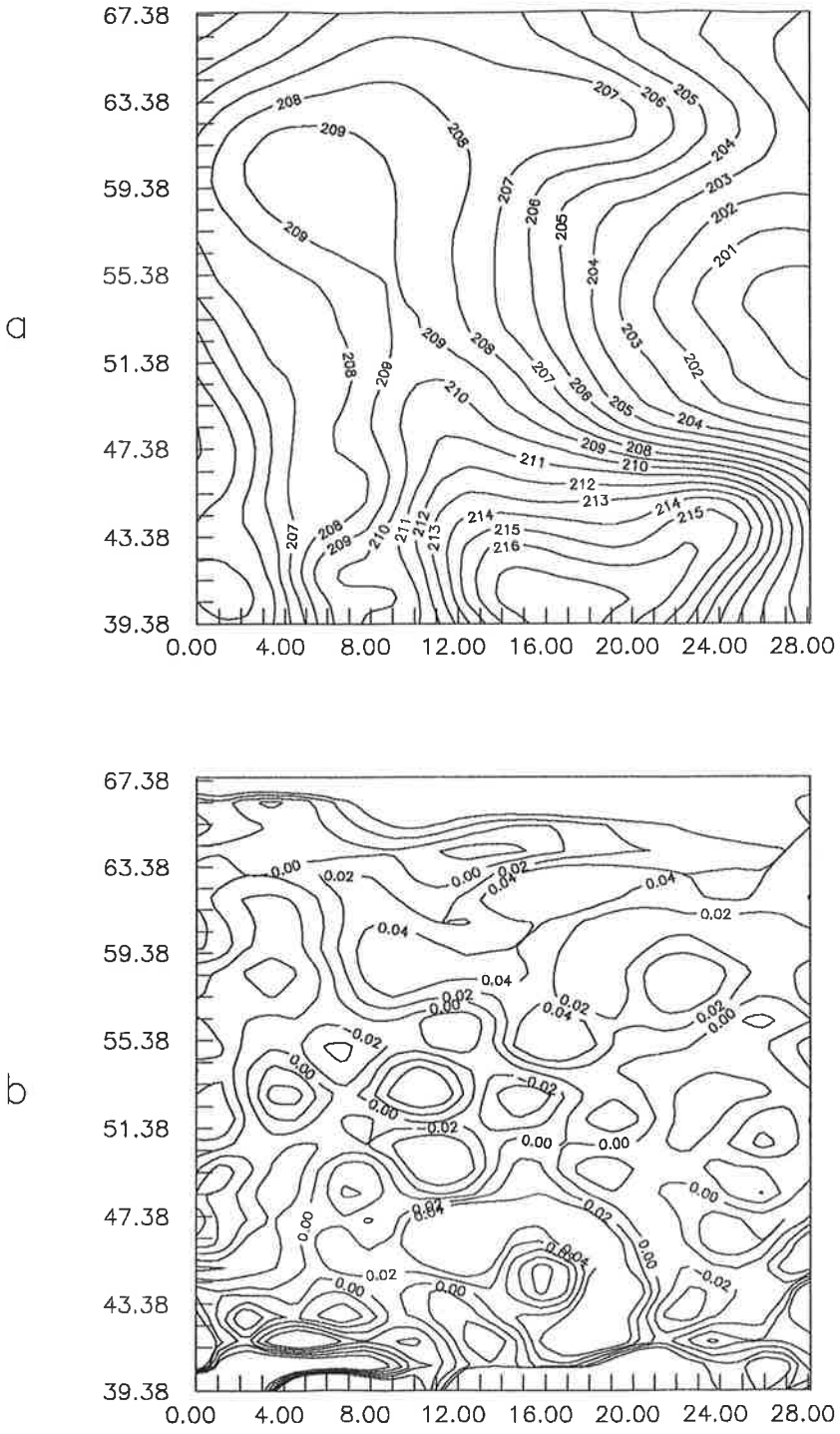

Fig. 29: European region: initial temperature (a) and its errors (b) for 200 mb pressure level.

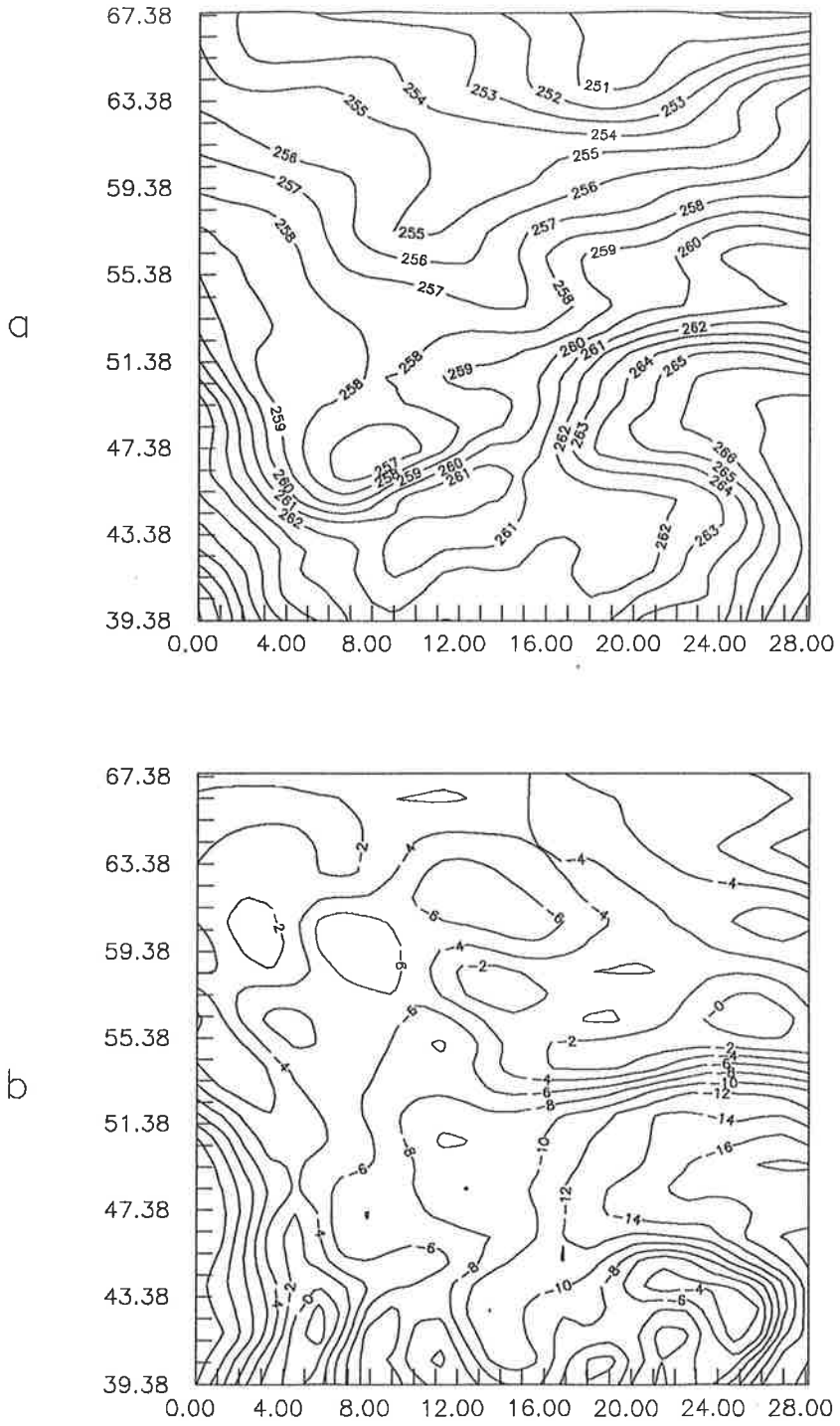

Fig. 30: European region: initial temperature (a) and its errors (b) for 700 mb pressure level.

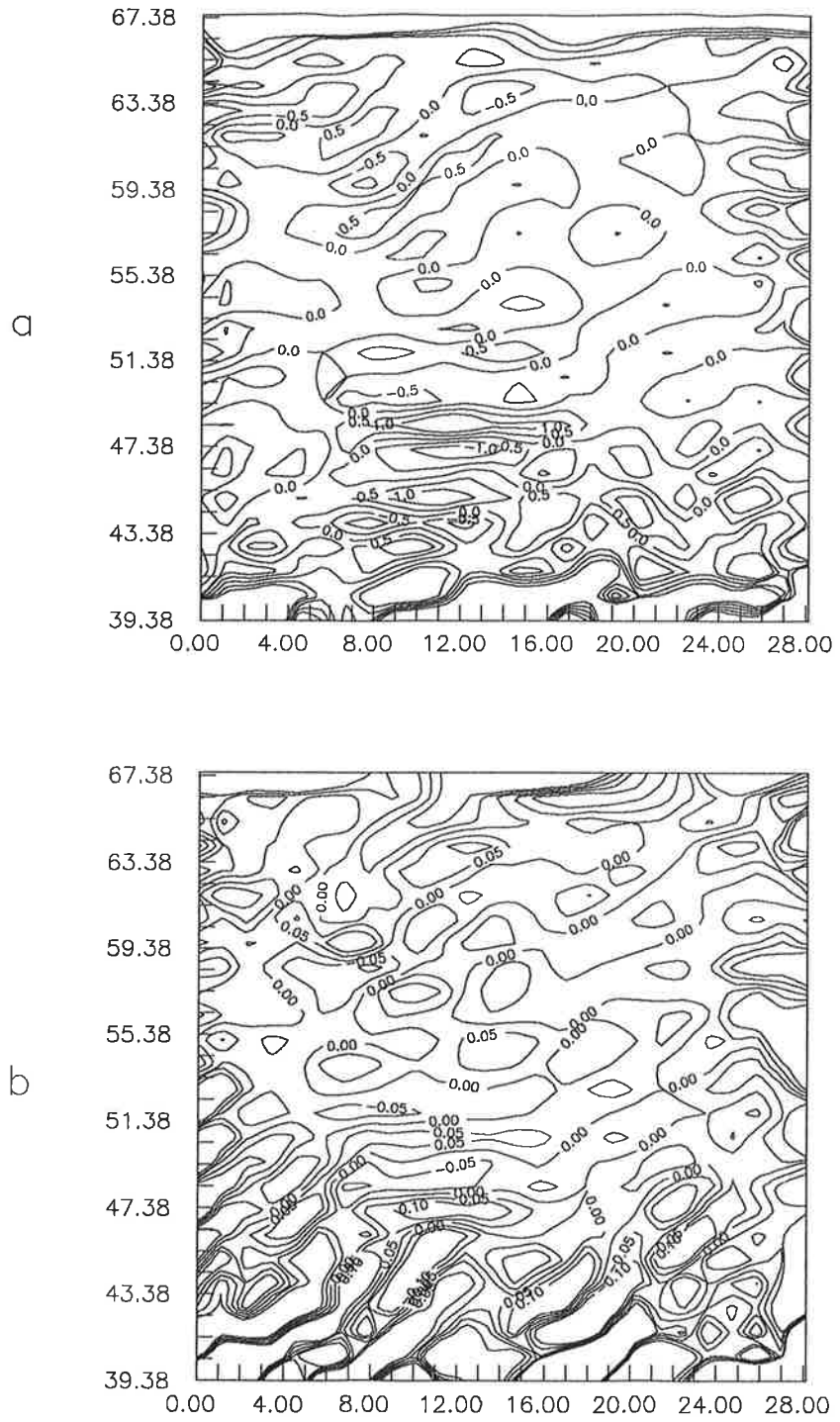

Fig. 31: European region: dry temperature error (a) and dry geopotential error (b) for 700 mb pressure level.

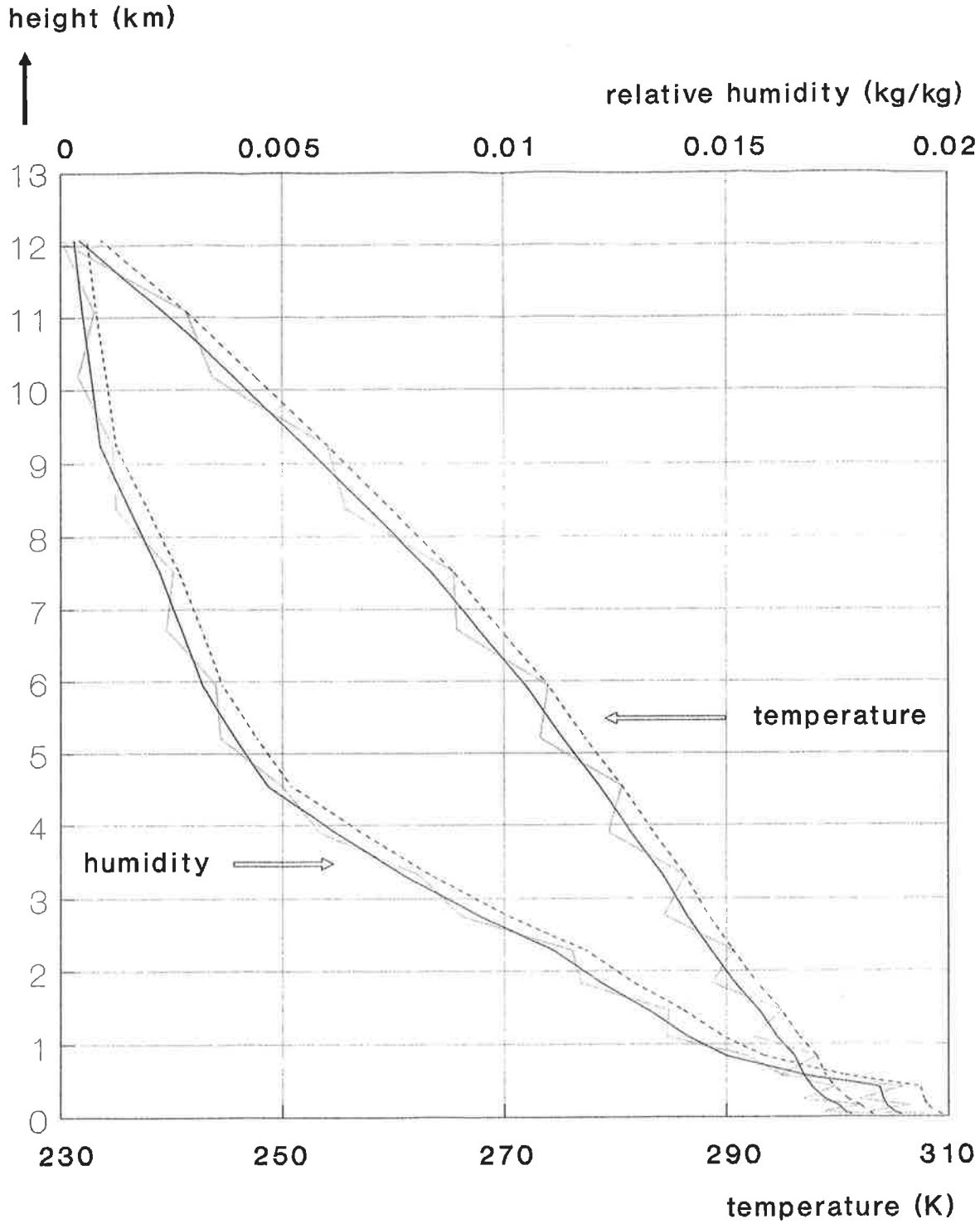

Fig. 32: An example of the retrieval of the vertical profile of specific humidity $q(z)$ from RF refractivity $n(z)$ and temperature $T(z)$.